Available online at www.sciencedirect.com
ScienceDirect
Geochimica et Cosmochimica Acta 70 (2006) 5990–6015
Geochimica
www.elsevier.com/locate/gca

# Feldspathic clasts in Yamato-86032: Remnants of the lunar crust with implications for its formation and impact history

L. Nyquist [a,*], D. Bogard [a], A. Yamaguchi [b,c], C.-Y. Shih [d], Y. Karouji [e], M. Ebihara [b,e], Y. Reese [f], D. Garrison [d], G. McKay [a], H. Takeda [g]

[a] *ARES, Mail Code KR, NASA Johnson Space Center, Houston, TX 77058, USA*
[b] *National Institute of Polar Research, Tokyo 173-8515, Japan*
[c] *Department of Polar Science, School of Multidisciplinary Science, Graduate University for Advanced Studies, Tokyo 173-8515, Japan*
[d] *Mail Code JE-23, ESCG/Jacobs Sverdrup, Houston, TX 77058, USA*
[e] *Department of Chemistry, Tokyo Metropolitan University, Hachioji, Tokyo 192-0397, Japan*
[f] *Mail Code JE-23, ESCG/Muniz Engineering, Houston, TX 77058, USA*
[g] *Research Institute, Chiba Institute of Technology, Narashino 257-0016, Japan*

Received 10 November 2005; accepted in revised form 31 July 2006

**Abstract**

Low concentrations of Th and Fe in the Yamato (Y)-86032 bulk meteorite support earlier suggestions that Y-86032 comes from a region of the moon far distant from the Procellarum KREEP Terrain (PKT), probably from the lunar farside. $^{39}Ar$–$^{40}Ar$, Rb–Sr, Sm–Nd, and Sm-isotopic studies characterize the chronology of Y-86032 and its precursors in the mega regolith. One of the rock types present in a light gray breccia lithology is an anorthosite characterized by plagioclase with An ~93, i.e., more sodic than lunar FANs, but with very low $^{87}Rb/^{86}Sr$ and $^{87}Sr/^{86}Sr$ similar to those of FANs. (FAN stands for Ferroan Anorthosite). This "An93 anorthosite" has Nd-isotopic systematics similar to those of nearside norites. A FAN-like "An97 anorthosite" is present in a second light-colored feldspathic breccia clast and has a more negative $\varepsilon_{Nd}$ value consistent with residence in a LREE-enriched environment as would be provided by an early plagioclase flotation crust on the Lunar Magma Ocean (LMO). This result contrasts with generally positive values of $\varepsilon_{Nd}$ for Apollo 16 FANs suggesting the possibility of assymetric development of the LMO. Other possible explanations for the dichotomy in $\varepsilon_{Nd}$ values are advanced in the text. The Y-86032 protolith formed at least 4.43 ± 0.03 Ga ago as determined from a Sm–Nd isochron for mineral fragments from the breccia clast composed predominantly of An93 anorthosite and a second clast of more varied composition. We interpret the mineral fragments as being predominatly from a cogenetic rock suite. An $^{39}Ar$–$^{40}Ar$ age of 4.36–4.41 ± 0.035 Ga for a third clast composed predominantly of An97 anorthosite supports an old age for the protolith. Initial $^{143}Nd/^{144}Nd$ in that clast was −0.64 ± 0.13 ε-units below $^{143}Nd/^{144}Nd$ in reservoirs having chondritic Sm/Nd ratios, consistent with prior fractionation of mafic cumulates from the LMO. A maximum in the $^{39}Ar$–$^{40}Ar$ age spectrum of 4.23 ± 0.03 Ga for a second sample of the same feldspathic breccia clast probably reflects some diffusive $^{40}Ar$ loss. Lack of solar wind and lunar atmosphere implanted Ar in the light gray breccia clast allows determination of an $^{39}Ar/^{40}Ar$ age of 4.10 ± 0.02 Ga, which is interpreted as the time of initial brecciation of this litholgy. After correction for implanted lunar atmosphere $^{40}Ar$, impact melt and dark regolith clasts give Ar ages of 3.8 ± 0.1 Ga implying melt formation and final breccia assembly ~3.8 Ga ago. Some breccia lithologies were exposed to thermal neutron fluences of $\sim 2 \times 10^{15}$ n/cm$^2$, only about 1% of the fluence experienced by some other lunar highlands meteorites. Other lithologies experienced neutron fluences of $\sim 1 \times 10^{15}$ n/cm$^2$. Thus, Y-86032 spent most of the time following final brecciation deeply buried in the megaregolith. The neutron fluence data are consistent with cosmogenic $^{38}Ar_{cos}$ cosmic ray exposure ages of ~10 Ma. Variations among differing lithologies in the amount of several regolith exposure indicators, including cosmogenic noble gas abundances, neutron capture induced variations in Sm isotopic abundances, and Ir contents, are consistent with a period of early (>~3.8 Ga ago) lunar regolith exposure, subsequent deep burial at >~5 m depth, and ejection from the moon ~7–10 Ma ago.


* Corresponding author. Fax: +1 281 483 1573.
*E-mail address:* laurence.e.nyquist@nasa.gov (L. Nyquist).

0016-7037/$ - see front matter © 2006 Elsevier Inc. All rights reserved.
doi:10.1016/j.gca.2006.07.042

## 1. Introduction

Lunar meteorites of predominantly feldspathic composition offer a much broader sampling of the early lunar crust than do Apollo- and Luna- returned samples, and almost certainly include material from the farside highlands. Consequently, such rocks yield additional insights into early lunar history. Yamato (Y)-86032 is a large (648 g) feldspathic lunar highland breccia composed of a variety of highland lithologies (Takeda et al., 1989; Koeberl et al., 1989; Takeda et al., 1990; Palme et al., 1991; Yamaguchi et al., 2004). One ancient feldspathic clast was found to have an Ar–Ar age of 4.35–4.41 Ga (Bogard et al., 2000a), and Sm–Nd isotopic systematics implying negative $\varepsilon_{Nd}$ at that time (Nyquist et al., 2002), suggesting a direct link to the primordial lunar magma ocean (LMO). Further, low concentrations of Th and Fe in Y-86032 suggest that it comes from a region of the moon that is far distant from the Procellarum KREEP Terrain (PKT) and the Apollo landing sites, perhaps from the farside of the Moon (Takeda et al., 1990; Karouji et al., 2004; Yamaguchi et al., 2004). Thus, Y-86032 provides an opportunity to study highland lithologies not sampled by the Apollo and Luna missions.

Eugster et al. (1989), Eugster (1989), and Vogt et al. (1991) determined cosmic ray exposure ages of ~10 Ma for Y-86032 and for paired meteorites Y-82192/3. However, as we will discuss in this paper, calculated cosmic ray exposure ages based on stable cosmogenic nuclides vary among different lithologies, and when combined with the corresponding thermalized secondary neutron fluences recorded in its clasts and impact melt matrix suggest a more complicated three-stage exposure history: (a) Early (pre 3.8 Ga) pre-exposure of regolith components in some lithologies; (b) Deep burial and shielding by several meters of megaregolith; (c) Exposure in space as a small body for 7–10 Ma.

The likely combination of lunar-farside and deep-megaregolith origin makes Y-86032 an extremely important, if complicated, lunar sample. Thus, we undertook a comprehensive combined mineralogical/petrographic, chemical, and chronological study of Y-86032 to better elucidate its history. Additional information about Y-86032 obtained by earlier consortium studies can be found in Takeda et al. (1989) and in other articles of the *Proceedings of the NIPR Symposium on Antartic Meteorites, No. 2*, as well as in later issues of the proceedings of NIPR symposia on Antarctic meteorites. Preliminary reports of the work presented here were given by Nyquist et al. (2005) and Yamaguchi et al. (2005).

## 2. Textural relationships and sample genealogy

A slab $(5.2 \times 3.6)$ cm$^2 \times 3$–5 mm thick was cut through the center of the meteorite (Fig. 1). We identified white (W) (~5 vol%), light gray (LG) (~20 vol%), dark gray (DG), and impact melt (IM) lithologies in the slab. The textural relationships among these lithologies are shown in Figs. 1 and 2. Fig. 2 shows that a fragment of the LG lithology was broken away and surrounded by the DG lithology during the brecciation event. Note also that the IM lithology smoothly abuts both of the other lithologies. W- and LG-clasts occur scattered throughout the DG and IM lithologies, and the LG lithology is itself brecciated. New samples representing the three main lithologies in the slab (LG, DG, and IM) were allocated for this study. The sample numbers and analytical program for each sample are summarized in Table 1. To insure close correlation between the petrographic and isotopic studies, eight Polished Thin Sections (PTSs) were made from representative portions adjacent to the samples used for chemical and isotopic studies, and PTS numbers are given in the table. The PTSs were examined by optical microscope, scanning electron microscope (SEM), and electron microprobe analyzers (EPMA) at the National Institute of Polar Research, Tokyo, the Ocean Research Institute of the University of Tokyo, and at the NASA Johnson Space Center, Houston, respectively. The chemical compositions of the various lithologies were analyzed by instrumental neutron activation analysis (INAA) and inductively coupled plasma mass spectrometry (ICP-MS) at Tokyo Metropolitan University. A preliminary report of the chemical data was given by Karouji et al. (2004).

We also report results for other samples of Y-86032. Samples Y-86032,116 and 117 studied by Nyquist et al. (2002) were produced from ,52, which is a remainder after separation of ,82 and ,83. A "gray clast" (GC) was extracted from Y-86032,116 for initial chronological studies. These samples are from the original sample of ,20 (original weight 6.90 g), which contained a large white (grayish) clast. The largest white clast in ,20 was separated as ,82 and the smaller one as ,83. Subamples of ,82 were studied by Tatsumoto and Premo (1991, sample ,118), Takaoka and Yosida (1992, sample ,108), and Kaneoka and Nagao (1993, sample ,92). The remainder was ,52, and appears to include a part of the white clast. Our PTS ,83-1 was made from a part of ,83. The preliminary examination report stated that thin section Y-86032,83-1 is a PTS of the large light clast in their Fig. 1 (Takeda et al., 1989). Electron probe microanalyses (EPMA) of PTS ,83-1, were made at the Ocean Research Institute, University of Tokyo, to support the work on ,116 (Takeda et al., 2002). Two additional PTSs were made of ,116 directly and studied by EPMA at the Johnson Space Center. Sample ,133 studied here was taken from sample ,52 and thus also is traceable to the original sample ,20 containing a portion of the large "light" clast of Fig. 1 of Takeda et al. (1989).

The white (W) slab lithology occurs as individual mm-sized clasts throughout the slab and must predate the other slab lithologies because it occurs within them. It was not possible to directly date the W lithology from clasts within the slab, but this lithology probably formed at the same time as the large clast (i.e., sample ,20) which it resembles petrographically and chemically, and thus at the same time as sample ,133 and sample ,116 GC. Sample ,116 GC has the oldest measured Ar–Ar age found for the Y-86032

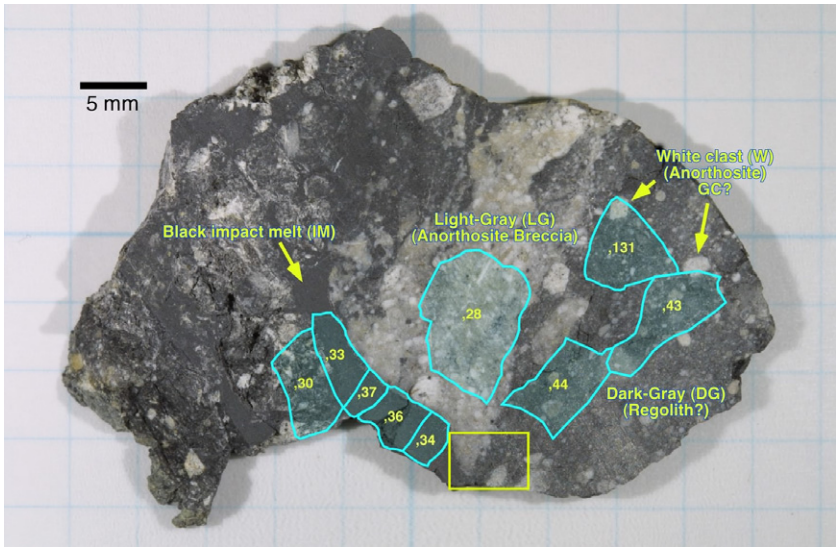


Fig. 1. Y-86032 slab from which samples were allocated for this investigation. Four lithologies were identified: White anorthositic or granulitic clasts (W), light gray anorthositic breccia (LG), dark gray regolithic breccia (DG), and black impact melt (IM). The sampled areas are outlined in blue. See Table 1 for a summary of the isotopic analyses for individual allocations. The relationships of IM and DG to LG within the outlined rectangular area are shown in more detail in the photomicrograph of Fig. 2.

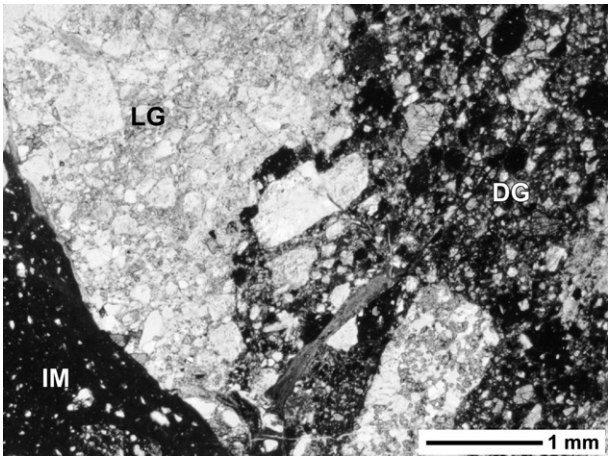


Fig. 2. Photomicrograph of Y-86032 showing the textures and relationships of the light gray (LG), dark gray (DG), and impact melt (IM) lithologies. Note that a fragment of the light gray (LG) lithology has broken away and has been surrounded by the dark gray (DG) lithology. Note also that the impact melt (IM) smoothly abuts both lithologies. Mineral clasts occur scattered throughout both the DG and IM lithologies.

clasts we studied. Its age of ~4.38 Ga is followed by that of sample ,133 for which the maximum Ar–Ar age is ~4.23 Ga. The lower age of sample ,133 suggests a greater degree of degassing of material perhaps similar in age to sample ,116 GC. The light-gray feldspathic breccia clast, ,28 LG, has a slightly younger Ar–Ar age of ~4.1 Ga, consistent with the presence of W lithology within it.

### 2.1. Textures and mineral chemistry

#### 2.1.1. Gray clast ,116 GC

In the Y-86032,83-1 PTS, we found three major lithologies: a light-colored feldspathic breccia clast, fragmental breccia matrices rich in mafic minerals, and a fragment-laden dark glassy breccia. The major lithic clast is $4.3 \times 3.8$ mm in size, and is a fine-grained light brown feldspathic breccia with subrounded plagioclase fragments. The largest fragment reaches up to $0.40 \times 0.19$ mm in size. The matrix is fairly uniform in texture and peppered with white spotty plagioclase and brownish glasses, but the shapes of mineral fragments are not clear. Under cross-polarized light, the matrices consist of very fine-grained plagioclase particles. The color of the matrices varies from brown to pale brown from place to place. Along the border with the glassy vein, the color of plagioclase matrices turned to white. Only one pyroxene grain was found in the gray clast and has the composition $Ca_3Mg_{58}Fe_{39}$, mg′ number ($Mg/(Mg + Fe) \times 100$ in molar units) = 60.

The An contents of the matrix plagioclase fragments range from An ~89 to An ~98.5 and plagioclase fragments in the gray clast range from An ~95.5 to An ~98. However, their most frequently observed compositions distribute within the same range, i.e., An ~96 to An ~97. These data suggest that the plagioclase fragments in the ,116 gray clast came from a single lithology, which is also the major lithic component of the place where this meteorite was ejected.

There is no indication in the mineralogical data that this gray clast contains anything but FAN (Ferroan Anorthosite) lithologies. One pyroxene (83-1 GC) found in the gray clast plots in the middle of the FAN trend (Fig. 3a) The textures and the presence of the brownish glass in the gray clast indicate granulation and sintering by an impact event. This texture is the same as is found in Y-82193 (Takeda et al., 1987) This observation suggests that its Ar–Ar age of ~4.4 Ga discussed later may represent the time of the impact.

Table 1
Y-86032 subsamples and analytical program

| Allocation | PTS | Discription | Analyses |
|---|---|---|---|
| Slab lithology | | | |
| Y-86032-,28 | 32, 45 | LG (light gray) | WR[a]: Ar–Ar, Sm IC[a], chem. comp., min seps: Rb–Sr, Sm–Nd |
| Y-86032-,30 | 31, 45 | IM (impact melt) | WR: Ar–Ar, Sm IC |
| Y-86032-,33 | | | WR: Ar–Ar, Rb–Sr, Sm–Nd, Sm IC |
| Y-86032-,34 | | IM (impact melt) | WR: chem. comp. |
| Y-86032-,36 | | IM (impact melt) | WR: chem. comp. |
| Y-86032-,37 | | IM (impact melt) | WR: Ar–Ar, Rb–Sr, Sm–Nd, Sm IC |
| Y-86032-,43 | 27, 45 | DG (dark gray) slab | WR: Sm IC min seps: Rb–Sr, Sm–Nd |
| Y-86032-,44 | | DG (dark gray) slab | WR: Sm IC min seps: Rb–Sr, Sm–Nd |
| Y-86032-,131 | | DG (dark gray) slab | WR: chem. comp. |
| Other samples from Y-86032 | | | |
| Y-86032-,116 | 83-1 | GC—light-colored clast<br>Matrix—darker portion of ,116 | WR: Ar–Ar, Rb–Sr, Sm–Nd, Sm IC |
| Y-86032-,133 | 83-1 | Light-colored clast | WR: Ar–Ar, Rb–Sr, Sm IC |

[a] WR = whole rock, IC = isotope dilution.

*2.1.2. Slab lithologies*

The W lithology in the slab occurs as rounded or subrounded clasts (up to 3 mm in size) of anorthosite with minor mafic minerals (<1–5 vol% on the slab). It includes a variety of feldspathic clasts such as feldspar fragments, granulitic clasts, and clasts similar to white portions in the LG lithology. The LG lithology is a breccia mostly composed of fragments of anorthosite (94.5%) with minor amounts (~5%) of pyroxene, olivine, silica minerals, and chromite. Olivine compositions are mostly $Fo_{78.1–82.4}$, but there are some relatively Fe-rich olivine grains ($Fo_{66.4–64.6}$). The compositions of pyroxene vary significantly: low-Ca (<5 mol% Ca) pyroxenes have mg′ = 41.0–81.3. Plagioclase compositions range from $An_{\sim 85.4}$ to $An_{\sim 96.6}$ with two peaks at $An_{\sim 88.5}$ and $An_{\sim 93}$. The peak at An ~93 is larger and contains ~91 vol% of the plagioclase grains (Fig. 3b). We also found a moderately brecciated clast, composed of plagioclase ($An_{86.0–90.9}$) and Fe-rich augite grains ($Wo_{41}En_{31}$) (<0.2 mm in size). On the An versus mg′ diagram (Fig. 3a), most of the minerals in this clast plot outside the regions of pristine nonmare rock groups, probably forming a different suite of igneous rocks (Yamaguchi et al., 2004). The LG lithology appears to be composed of fragments from volumetrically minor augite-bearing rocks with plagioclase of $\sim An_{88.5}$ plus rocks with more An-rich plagioclases and more Mg-rich mafic minerals. The rocks thus represented may form a related suite of igneous rocks.

The DG lithology is a dark matrix composed of a variety of clast types: fragments of feldspathic clasts (W lithology), glassy (impact melt) clasts, granulitic clasts, basaltic clasts, and mineral fragments. Olivine compositions vary from $Fo_{5–83}$, and the mg′ of pyroxenes varies in the range 38.3–81.2. Plagioclase compositions are $An_{68.8–97.9}$. In Fig. 3a, a granulitic clast (Gr) and an anorthositic clast (Ano) plot between the FAN and Mg-suite fields, like clasts in the Apollo granulites (Lindstrom and Lindstrom, 1986). A basaltic clast (0.40 × 0.38 mm in size) in the DG lithology is composed of zoned pyroxene and plagioclase with minor amounts of silica minerals and Ti-rich phases. There are also fragments of mafic minerals that could be derived from mare basalts. The grain boundaries of clasts and mineral fragments are cemented by very fine vesiculated intergranular melts.

The impact melt (IM) vein is a dark glassy matrix with various kinds of lithic and mineral fragments similar to those in the DG lithology. The sizes of fragments in the glass are smaller than those in the DG matrix and they are more rounded. The textural observations suggest that Y-86032 is a breccia resulting from at least two impact events. During the first event, the LG breccia was incorporated into the DG matrix, and during the second event both lithologies were shear-deformed and cut by IM veins. Since the LG-lithology is itself brecciated, a third, prior impact event also may have occurred. The presence of vesiculated intergranular melts in the DG lithologies suggests peak shock pressures of ~10–15 GPa (Bischoff and Stöffler, 1992). Although temperatures were locally more than ~1600 °C, the bulk temperatures were no more than several hundred °C judging from the small amounts of melts present. The breccia was shocked again after initial formation, and impact melt veins (~20–30 vol%) formed locally. After thermal equilibration, the bulk temperature would have increased to >400 °C. These shock events could have partially reset some of the Ar–Ar ages. As shown below, the range of Ar–Ar ages of the lithologies implies at least two and possibly three impact heating events.

## 3. Chemical composition of the Y-86032 lithologies

The average bulk composition of the three main lithologies of Y-86032 (Table 2, column 1) is consistent with previous analyses of this meteorite (column 3, Koeberl et al., 1989; Palme et al., 1991; Korotev et al., 1996), except that $Al_2O_3$, $Na_2O$, $K_2O$, Ba, and Eu are higher for the average of our samples, and $TiO_2$, FeO, $Cr_2O_3$, Heavy Rare Earth Elements (HREEs) and siderophile elements are lower.

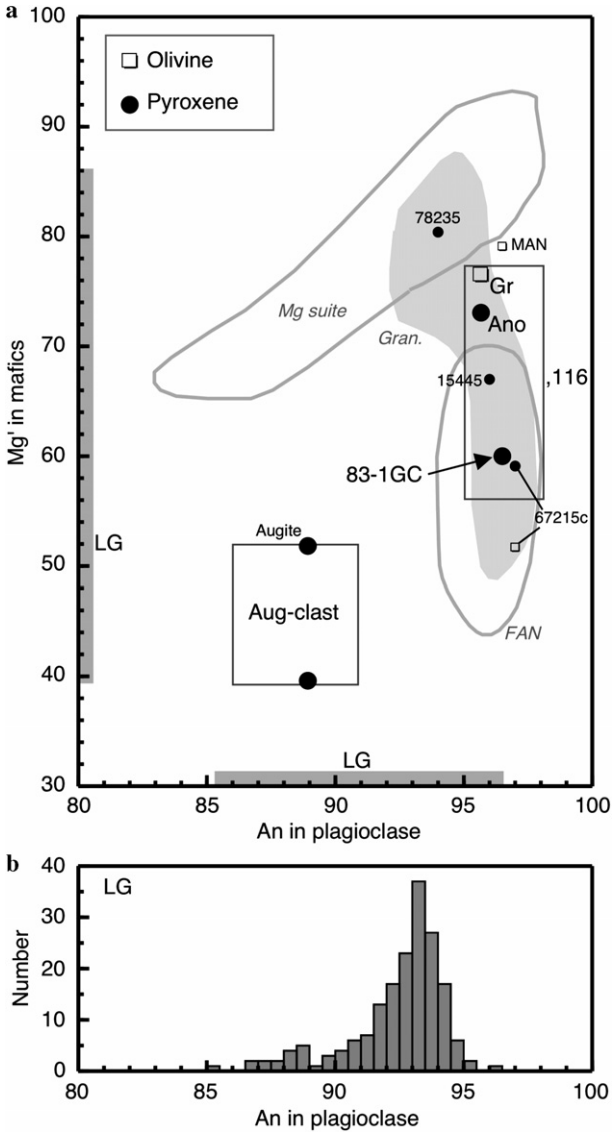


Fig. 3. (a) Plot of mg′ in mafic minerals vs. An in plagioclase. Data for "Aug-clast" are for an augite-bearing clast from the light-gray lithology. "Gr" and "Ano" are fragments of granulite and anorthosite from the dark-gray lithology, respectively. Bars labeled LG show the ranges of compositions of plagioclase and low-Ca pyroxene in the light gray (LG) lithology. Shaded and outlined areas are for the pristine rock suites and granulites (Lindstrom and Lindstrom, 1986). Data for ~4.4 Ga old pristine highland rocks 15445, 67215c, and 78235 are from Ridley et al. (1973), Norman et al. (2003), and McCallum and Mathez (1975), respectively. The datum for the Magnesian Anorthosite from Dhofar 489 (MAN) is from Takeda et al. (2006). (b) Histogram of plagioclase compositions from analyses of the LG lithology.

These differences reflect a greater contribution of the anorthositic LG breccia to the numerical average of column 1 than to the bulk analyses of Y-86032 averaged for column 3. The lower standard deviation values of column 4 than those of column 2 indicate that most other labs analyzed well-mixed matrix material. Higher values (except for $Al_2O_3$ and Gd) of column 2 than those of column 4 indicate that the chemical compositions of the three different textural materials analysed in this investigation are variable. The FeO content of the LG breccia (2.37 wt% (Karouji, pers. comm.); *cf.* Fig. 4) not only is lower than that of other Y-86032 lithologies, it also is lower than that of other lunar feldspathic meteorites (Korotev et al., 2003a,b, Fig. 4). The slight differences in the average compositions of Y-86032 and the paired meteorites Y-82192/3 (columns 5 and 6 of Table 2) are mostly consistent with the trend established between the numerical and bulk averages of Y-86032: There are slight enrichments of the plagiophile elements $Al_2O_3$, CaO, and Eu in Y-86032 compared to Y-82192/3.

Warren and Wasson (1977) suggest that siderophile element contents $<3\times10^{-4}$ times those of CI chondrites (~0.12 ppb) provide the most reliable evidence for pristinity. The Ir contents of LG, DG, and IM are significantly higher than this limit, consistent with the textural evidence for multiple impacts. Ir abundances are variable among the slab lithologies, being 5.7 ppb and 9.3 ppb in two different samples of IM and 9.3 ppb in DG, but only 1.8 ppb for LG (Karouji, pers. comm.). The average Ir content of 6.5 ppb, (Table 2, column 1) is typical of feldspathic lunar meteorites (Korotev et al., 2003a,b; Fig. 8), and can be explained by meteoritic contamination.

In spite of the petrographic evidence of impact mixing, the Y-86032 subsamples have very low Th (average = 0.156 ppm (Table 2); slab range = 0.0765–0.191 ppm (Karouji, pers. comm.)) and U (average = 0.0468 ppm; slab range = 0.0258–0.0564 ppm (Karouji, pers. comm.). These low abundances confirm the absence of KREEP components. The average Th and Sm abundances of Y-86032 place it among the most KREEP-poor lunar highlands meteorites (*cf.* Fig. 10 of Korotev (2005)). Coupled with the low FeO contents, these data are consistent with a lunar farside origin for Y-86032. It usually is argued that the bulk compositions of regolith breccias can be directly compared with remote sensing data, e.g., with the lunar Th map, because regolith breccias are composed of fine-grained clasts and fragments and are well-mixed. Thus, the bulk compositions of the breccias represent relatively large areas of the lunar surface that are comparable to the resolution of the remote sensing data, and low Th concentration in fine-grained, well-mixed breccias becomes evidence that the breccias are derived from a low Th area (e.g., the lunar farside). Although Y-86032 is not a regolith breccia, its DG lithology is well-mixed and composed of relatively fine-grained materials including a variety of highland rocks, impact melts, basalts, etc. We argue later in the paper that the Y-86032 breccia was assembled ~3.8 Ga ago, and that the duration of near-surface exposure prior to that time was limited, but residence of its constituent lithologies in the megaregolith prior to consolidation makes it reasonable to conclude that the Y-86032 breccia was derived from a Th-poor region of the Moon. The average Th and FeO concentrations of Y-86032 fall within the elliptical region for feldspathic lunar meteorites shown in Fig. 15. of Korotev (2005). Average FeO of ~4% places it near the maximum of the frequency distribution of FeO values as observed from orbit by the Clementine space craft shown in the same figure suggesting

Table 2
Chemical compositions of Yamato 86032 and Yamato 82192/3

| | Y-86032 | | | | Y-82192 | Y-82193 |
|---|---|---|---|---|---|---|
| | [1] | [2] | [3] | [4] | [5] | [6] |
| $SiO_2$ (%) | 44.9 | 0.8 | 44.6 | 0.6 | 45.8 | 44.5 |
| $TiO_2$ (%) | 0.181 | 0.048 | 0.200 | 0.025 | 0.32 | 0.23 |
| $Al_2O_3$ (%) | 29.6 | 1.1 | 28.5 | 1.2 | 26.3 | 26.7 |
| $Cr_2O_3$ (%) | 0.0823 | 0.0321 | 0.0985 | 0.0052 | 0.138 | 0.127 |
| FeO (%) | 4.06 | 1.16 | 4.28 | 0.18 | 5.47 | 4.97 |
| MnO (%) | 0.0624 | 0.0170 | 0.0607 | 0.0042 | 0.0821 | 0.0704 |
| MgO (%) | 5.10 | 1.43 | 5.36 | 0.48 | 5.41 | 5.55 |
| CaO (%) | 16.4 | 1.8 | 16.0 | 0.3 | 12.71 | 16.23 |
| $Na_2O$ (%) | 0.557 | 0.117 | 0.450 | 0.032 | 0.402 | 0.416 |
| $K_2O$ (%) | 0.039 | 0.012 | 0.020 | 0.005 | 0.040 | 0.029 |
| Total (%) | 101.0 | | 99.6 | | 96.6 | 98.9 |
| Sc (μg/g) | 8.34 | 2.92 | 8.30 | 0.39 | 12.02 | 9.95 |
| V (μg/g) | 27.2 | 11.4 | 26.0 | 4.3 | 36.35 | 31 |
| Co (μg/g) | 13.3 | 4.4 | 14.7 | 1.2 | 16.9 | 17.6 |
| Ni (μg/g) | 97.1 | 43.5 | 130 | 22 | 129 | 145 |
| Ba (μg/g) | 39.6 | 10.5 | 24.4 | 1.7 | 23.0 | 28.0 |
| La (μg/g) | 1.20 | 0.22 | 1.30 | 0.14 | 1.16 | 1.30 |
| Ce (μg/g) | 2.93 | 0.59 | 3.37 | 0.39 | 2.94 | 3.45 |
| Pr (μg/g) | 0.428 | 0.098 | 0.45 | | 0.32 | |
| Nd (μg/g) | 1.86 | 0.43 | 2.01 | 0.22 | 1.86 | 2.00 |
| Sm (μg/g) | 0.561 | 0.143 | 0.602 | 0.04 | 0.583 | 0.620 |
| Eu (μg/g) | 1.01 | 0.15 | 0.928 | 0.11 | 0.830 | 0.875 |
| Gd (μg/g) | 0.681 | 0.206 | 0.847 | 0.25 | 0.707 | 0.570 |
| Tb (μg/g) | 0.125 | 0.039 | 0.132 | 0.01 | 0.147 | 0.145 |
| Dy (μg/g) | 0.843 | 0.287 | 0.996 | 0.14 | 1.012 | 0.865 |
| Ho (μg/g) | 0.186 | 0.062 | 0.210 | 0.03 | 0.221 | 0.170 |
| Er (μg/g) | 0.544 | 0.193 | 0.61 | | 0.510 | |
| Tm (μg/g) | 0.0805 | 0.0292 | 0.112 | 0.01 | 0.091 | |
| Yb (μg/g) | 0.543 | 0.189 | 0.583 | 0.02 | 0.632 | 0.645 |
| Lu (μg/g) | 0.0795 | 0.0284 | 0.0842 | 0.004 | 0.0963 | 0.0985 |
| Hf (μg/g) | 0.402 | 0.045 | 0.426 | 0.044 | 0.501 | 0.435 |
| Ir (ng/g) | 6.5 | 3.6 | 5.3 | 0.9 | 5.3 | 5.9 |
| Th (μg/g) | 0.156 | 0.054 | 0.198 | 0.03 | 0.160 | 0.195 |
| U (μg/g) | 0.0468 | 0.0141 | 0.0534 | 0.007 | 0.0478 | 0.0485 |

[1]The average composition of 3 main lithologies (LG, DG and IM) of Y-86032. [2]The standard deviation ($1\sigma$) of the average of analyses of ,28LG (481 mg) ,34IM (82 mg) ,36IM (91 mg) and ,131DG (237 mg). [3]Mean calculated from data in Fukuoka et al. (1989), Koeberl et al. (1989), Korotev et al. (1996), Palme et al. (1991), Warren and Kallemeyn (1991). [4]The standard deviation ($1\sigma$) for previous data. [5]Mean calculated from data in Bischoff et al. (1987), Fukuoka et al. (1986), Koeberl (1988), Lindstrom et al. (1991), Palme et al. (1991), Warren and Kallemeyn (1991). [6]Mean calculated from data in Fukuoka et al. (1986), Warren and Kallemeyn (1991).

that Y-86032 is from a typical region of the lunar feldspathic highlands.

Fig. 4 shows that the Th and FeO concentrations in Y-86032 are comparable to those in some ancient, pristine lunar highland rocks. Of these, ~4.4 Ga old anorthosite 67215 and norite 78235 are displaced towards higher FeO and Th values, respectively, than are the data for feldspathic lunar meteorites. Korotev (2005, Fig. 15) notes that the modal Th abundance in the feldspathic highlands is 0.7 ppm. The low Th contents of the Y-86032 lithologies, and especially of the LG lithology, suggest that contributions of rocks like the Mg-suite norites of the Apollo collection to the Y-86032 site must have been limited. It has been argued that norites and other Mg-suite rocks in the Apollo collection are associated only with the Procellarum KREEP Terrain (PKT) (Korotev, 2005). One of the reasons cited by Korotev (2005) for concluding that such Mg-suite rocks are absent from ''true'' highlands is their rarity as clasts in the lunar meteorites. However, Korotev (p. comm.) notes that some feldspathic lunar meteorites do contain magnesian (high Mg/Fe) anorthosites and troctolitic anorthosites. Also, Takeda et al. (2006) observed a spinel troctolite clast with An ~96 in the Dhofar 489 lunar meteorite. They suggest that such spinel troctolites may be part of a farside lunar differentiation trend. Only slightly lower An ~95 and mg′ ~88 in troctolite 76535 shown in Fig. 4 suggests it is relatively primitive, rivaling some FANs in An content. However, it probably crystallized from a parent magma of moderately high trace element content (Haskin et al., 1974) consistent with its derivation from the PKT. The observation that average Th (and REE) are much lower in Y-86032 than in Apollo collection norites suggests that Y-86032 originated far from the provenance of such norites, i.e., far from the PKT. The Th abundance in LG is lower even than in the 76535 troctolite. The unique composition of the LG clast lithology, the

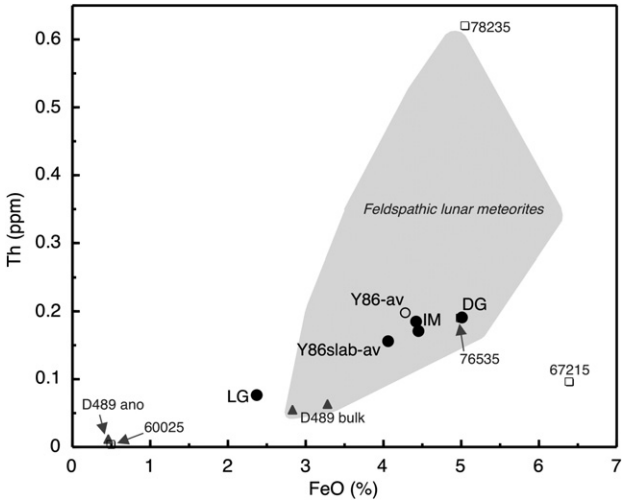


Fig. 4. FeO–Th diagram of Y-86032 from data reported by Karouji et al. (2004) (DG, IM) and Karouji, pers. comm. (LG). Sample allocations for LG, DG, and IM are identified in Table 1. Compositional range of feldspathic lunar meteorites is shown as a shaded area (Korotev et al., 2003a,b). Compositions of Dho 489 and Dho 489 anorthosite are from Takeda et al. (2006). Data for ~4.4 Ga old ferroan anorthosites 60025 and 67215c, as well as ~4.3–4.4 Ga norite 78235 and troctolite 76535 are also shown for comparison. The Th concentration in 60025 was estimated as ~4× the U concentration (Krahenbuhl et al., 1973).

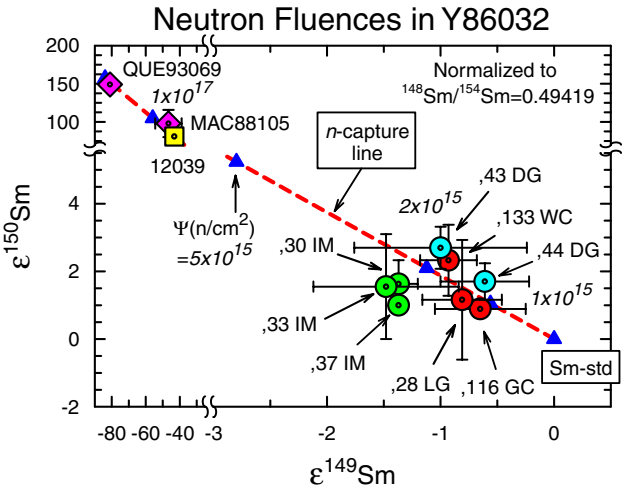


Fig. 5. Sm isotopic composition of Y-86032 subsamples. The data are tightly clustered, nearly overlapping within analytical uncertainty, but three samples (,116GC ,28LG and ,44DG) cluster to the right on the diagram (lowest neutron exposure) and three samples (,30 IM ,33 IM and ,30 IM) cluster to the left (highest neutron exposure). The subsample of allocation ,30 DG that was analysed for Sm isotopes was enriched in impact melt, and is here designated IM. Those samples most enriched in light-colored, feldspathic clasts appear to have the lowest exposure to thermal neutrons, and, thus, the shortest regolith residence time. Note that ,44 DG from which minerals were separated for the Sm–Nd isochron, is among those samples showing the lowest neutron exposure. The comparatively large mineral clasts separated from this regolith sample had minimal regolith exposure. (For interpretation of the references to color in this figure legend, the reader is referred to the web version of this paper.)

presence of a hitherto unknown augite-bearing clast type within it, and the Nd- and Sr- isotopic data presented later in the paper all provide additional arguments for a farside origin of Y-86032.

## 4. Sm isotopic composition of Y-86032 lithologies

The Sm isotopic compositions were measured for all allocations of the Y-86032 lithologies, and show small variations from the composition of the terrestrial isotopic standard due to capture of thermalized neutrons. Neutron-capture induced variations in $^{149}$Sm and $^{150}$Sm are given in $\varepsilon$-units (parts in $10^4$) in Table 3 and Fig. 5. Sm analyses of sample ,116 GC were normalized to $^{147}Sm/^{152}Sm = 0.56081$ (Wasserburg et al., 1981). However, because of neutron capture on $^{151}$Eu , normalizing to $^{152}$Sm is not a good choice for lunar highland samples with large Eu/Sm ratios, i.e., large positive Eu anomalies. This was not a significant problem for sample ,116 GC because the secondary neutron fluence experienced by this sample was low enough so that the effect on the Sm-isotopic composition was insignificant. $^{152}$Sm was not used for normalization for the other Y-86032 lithologies. Furthermore, an unidentified interference at mass-147 made $^{147}$Sm inappropriate for normalization. This effect was most noticeable for ,37 IM for which the mass-147 interference was nearly 5 $\varepsilon$-units, as shown by renormalizing to $^{148}Sm/^{154}Sm = 0.49419$ (Wasserburg et al., 1981). We do not assign formal error limits to the ,37 IM data in Table 3 because small interferences also may have been present for other masses in addition to mass-147. An exponential mass-fractionation law was assumed for normalization of the measured Sm-isotopic composition to $^{147}Sm/^{152}Sm$ or $^{148}Sm/^{154}Sm$, respectively.

Table 3
Thermal neutron capture effects on $^{149}$Sm and $^{150}$Sm in Y-86032 lithologies

| Sample | $\varepsilon^{149}Sm$[a] | $\pm2\sigma_m$[b] | $\varepsilon^{150}Sm$[a] | $\pm2\sigma_m$[b] | $\Psi$ (n/cm$^2$) × $10^{15}$ |
|---|---|---|---|---|---|
| ,28LG | −0.81 | 0.35 | 1.16 | 1.77 | 1.23 |
| ,133WC | −0.93 | 0.25 | 2.33 | 1.05 | 2.03 |
| ,43DG | −1.00 | 0.76 | 2.70 | 0.62 | 2.31 |
| ,44DG | −0.61 | 0.39 | 1.70 | 0.54 | 1.44 |
| ,30IM | −1.37 | 0.17 | 1.63 | 0.70 | 1.87 |
| ,37IM | −1.37 | 1.00 | 1.00 | 0.92 | 1.48 |
| ,33IM | −1.48 | 0.64 | 1.55 | 1.55 | 1.89 |
| ,116GC | −0.66 | 0.41 | 0.90 | 0.11 | 0.97 |

[a] Normalized to $^{148}Sm/^{154}Sm = 0.49419$ or $^{147}Sm/^{152}Sm = 0.56081$ (Wasserburg et al., 1981).
[b] Uncertainties are twice the standard deviation of the mean for 2 to 5 individual analyses.

In Fig. 5 all of the $\varepsilon^{149}$Sm and $\varepsilon^{150}$Sm values lie within analytical uncertainty of the n-capture line for conversion of $^{149}$Sm to $^{150}$Sm. Neutron fluences calculated following the method of Lingenfelter et al. (1972) are shown in the last column of Table 3. For these calculations, the average chemical composition of the three main lithologies of Y-86032 (Table 2) was used to determine the total macroscopic thermal neutron cross section at the Y-86032 site. The effective thermal neutron cross section thus calculated is $\sigma_{Th} = 5.58 \times 10^{-20}$ cm$^2$. The total neutron fluence, $\Psi$ (n/cm$^2$) experienced by each sample was calculated from the relationship between $\Psi$, $\sigma_{Th}$, and the $^{150}$Sm/$^{149}$Sm ratio in irradiated and unirradiated samples given by Russ et al. (1971). In terms of the directly measured $\varepsilon$-values:

$$\Psi \sim 0.348\sigma_{Th}^{-1}[(1 + 10^{-4}\varepsilon^{150}\mathrm{Sm})/(1 + 10^{-4}\varepsilon^{149}\mathrm{Sm}) - 1]. \quad (1)$$

In deriving this simplified form we have substituted numerical values for the isotopic composition of the terrestrial standard; i.e., $^{150}$Sm/$^{154}$Sm = 0.32440, $^{149}$Sm/$^{154}$Sm = 0.60746, and $^{150}$Sm/$^{149}$Sm = 0.53402. Furthermore, we have used the approximation $[(1 + 10^{-4}\ \varepsilon^{150}\mathrm{Sm})/(1 + 10^{-4}\ \varepsilon^{149}\mathrm{Sm}) \sim 1$ when added to the constant value 1.87. The percentage error introduced into the sum and thereby into $\Psi$ by this approximation is insignificant.

The total neutron fluence experienced by ,28 LG and ,116 GC was $\sim 1 \times 10^{15}$ n/cm$^2$ (Table 2 and Fig. 5). The other lithologies experienced fluences ranging up to about twice as great. The fluences experienced by the Y-86032 lithologies are about 100-fold less than for lunar highland regolith meteorites MAC88105 and QUE93069, for example, and also are significantly less than for most Apollo returned samples. Of the 14 mare basalts for which Nyquist et al. (1995) reported Sm-isotopic data, only three of them have neutron-capture induced $^{149}$Sm anomalies of $<\sim -1$ $\varepsilon$-unit: 70135, 74255, and lunar meteorite Asuka-881757. Of these, $\varepsilon^{149}\mathrm{Sm} = -1.2 \pm 0.4$ for basalt 70135 is a close match to the least-exposed Y-86032 lithologies. Arvidson et al. (1976) reported a $^{81}$Kr–Kr exposure age of $106 \pm 4$ Ma for 70135 and suggested that this age possibly correlated with an influx of crater debris from the crater Tycho near the Apollo 17 site. Thus, 70135 probably experienced a lunar surface, single-stage irradiation. The comparable neutron fluence experienced by the Y-86032 lithologies, but much younger noble gas exposure ages of $\sim$10 Ma (presented later) suggest that most of their exposure to thermal neutrons occurred at greater regolith depths than for 70135, which probably always resided at shallow depths above the buildup of the secondary neutron flux.

Another comparison is provided by the Chico and Torino meteorites, which experienced thermal neutron fluences of $\sim 10^{16}$ n/cm$^2$ and have exposure ages of $\sim$60–65 Ma (Bogard et al., 1995). Since both the noble gas exposure age and the thermal neutron fluence of the Y-86032 lithologies are proportionally less, one may infer that Y-86032, Chico, and Torino were approximately similarly shielded. That is, for Chico, cosmogenic nuclides indicate a pre-atmospheric meteoroid radius of $\sim$50–100 cm, a nominal single-stage exposure age of 65 Ma, and a neutron fluence of $1.23 \pm 0.06 \times 10^{16}$ n/cm$^2$ (Bogard et al., 1995) indicating a flux of $\sim 1.9 \times 10^{14}$ n/cm$^2$ Ma$^{-1}$. Similarly for Torino, a single-stage exposure age of $\sim$60 Ma and a neutron fluence of $0.84 \pm 0.06 \times 10^{16}$ n/cm$^2$ (Bogard et al., 1995) indicate a neutron flux of $\sim 1.4 \times 10^{14}$ n/cm$^2$ Ma$^{-1}$. The greater abundance of neutron absorbers in L-chondrites compared to lunar highland rocks results in a higher effective capture cross section $\sigma_{Th} = 6.4 \times 10^{-20}$ cm$^2$ (see Bogard et al., 1995) compared to $\sigma_{Th} = 5.58 \times 10^{-20}$ cm$^2$ for Y-86032. Assuming an average flux of $\sim 1.65 \times 10^{14}$ n/cm$^2$ Ma$^{-1}$ and correcting for the difference in effective cross sections suggests nominal $4\pi$ "neutron exposure ages" for the Y-86032 lithologies ranging from $\sim$7 Ma for ,116 GC to $\sim$16 Ma for ,43 DG. If most of the neutron irradiation occurred on the lunar surface ($2\pi$ irradiation), the exposure ages would be twice as long.

Neglecting the less reliable ,37 IM analysis, neutron fluences of $\sim 1.9 \times 10^{15}$ n/cm$^2$ are calculated for the two other impact melt samples, about twice the values for ,28 LG and ,116 DG. The average neutron fluence calculated for the two DG regolith samples also is $\sim 1.9 \times 10^{15}$ n/cm$^2$. The white clast lithology ,133 WC also experienced a neutron fluence of $\sim 2.0 \times 10^{15}$ n/cm$^2$. That the impact melt and DG samples experienced slightly higher neutron fluences than the light gray lithology is qualitatively consistent with their longer regolith residence times as implied by higher Ir contents. (We note that our allocation of ,30 consisted of an intimate mixture of IM and LG lithologies (*cf.* Fig. 1), and that the Sm-isotopic data were obtained on dominantly IM lithology, whereas the $^{39}$Ar–$^{40}$Ar data reported below are for a sample of dominantly LG lithology.) That the neutron fluence recorded by ,133 WC was comparable to that recorded by the DG and IM lithologies suggests that its immediate precursor existed as a smallish rock in the regolith prior to final brecciation.

The Sm isotopic data thus are consistent with a relatively simple scenario in which the little-exposed LG lithology was engulfed during initial brecciation by DG regolith material having greater exposure to thermal neutrons and meteoritic contamination. Introduction of impact melt during final brecciation, as suggested by the textural observation, could have occurred soon thereafter, which would also be consistent with the close compositional similarity between the IM and DG material.

## 5. Chronology of Y-86032

### 5.1. Sm–Nd age

#### 5.1.1. Relation of mineral separates to mineralogy

Because the chronological studies do not utilize *in situ* techniques, a precise correlation of the isotopic data to sample mineralogy is not possible. Nevertheless, because

of the absence of KREEP or other trace element rich components in the protolith(s) of the Y-86032 clast lithologies, and because of the low trace element abundances in olivine, the primary contributors in the protolithic rock suite to the isotopic data must be plagioclase and pyroxene. For the Sm–Nd and Rb–Sr isotopic studies, these two minerals were separated from bulk clastic material according to their differing densities.

Fig. 6 shows the separation procedures for the ,28 LG clast; procedures used for ,44 DG material were similar. In each case, the starting material for the separation procedures was ground to a grain size <75 μm. The grain size of mineral clasts in LG are variable in the range ~30–250 μm. Thus, the grain size used for mineral separation was comparable to or less than the size of typical mineral clasts in ,28 LG. A first separation was made at a density of 2.85 g/cm$^3$. The lighter fraction was dominantly plagioclase, part of which was saved, and part analysed. The denser fraction was separated again at 3.32 g/cm$^3$, to obtain samples labeled Px1 and Px2, respectively. The denser separate was the purest pyroxene, and for ,28, comprised only ~3% of the starting material by weight. These mineral separate yields can be compared to the modal abundances of anorthite (94.5%) with minor amounts (~5%) of pyroxene, olivine, silica minerals, and chromite. Of the minerals in the mode, anorthite and silica would go into the lighter (<2.85 g/cm$^3$) fractions, whereas pyroxene, olivine and chromite would go into the fraction >3.32 g/cm$^3$, i.e., the fraction labeled Px2. The "Px1" fraction of intermediate density (2.85–3.32 g/cm$^3$) likely contains some anorthite as well as mafic minerals because the combined weight (Px1 + Px2) is 9.5% of the total, which exceeds the petrographically observed modal abundance of mafic minerals in ,28. Fig. 7 shows that the heavier Px2 samples from both the LG-lithology ,28 and the DG-lithology ,44 were distinctly enriched in Sm and Nd abundances compared to bulk samples, displaying the HREE enrichment and LREE depletion characteristic of pyroxene. Because the Px2 samples have the largest Sm/Nd ratio, they are the ones that most determine the Sm–Nd age.

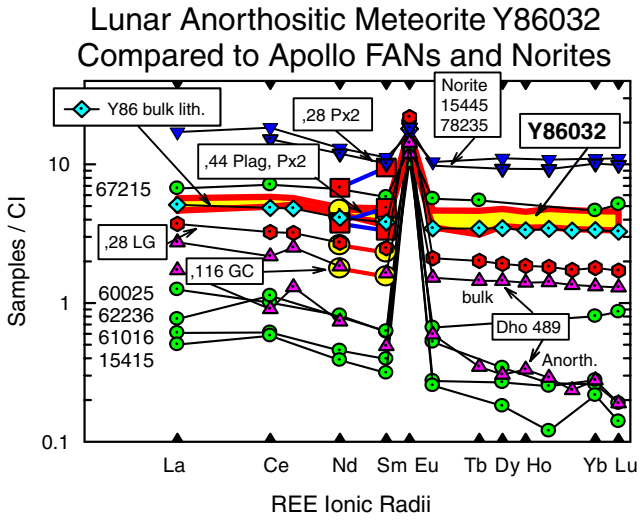


Fig. 7. Sm and Nd abundances in Y-86032 mineral separates compared to those in bulk samples and to the overall REE abundance patterns of Y-86032 lithologies, Apollo FANs, magnesian anorthosite Dho 489 and the "d2" anorthositic clast in it (Takeda et al., 2006), norite 78235, and a noritic clast from 15445. Apollo sample data are from the literature. Sm and Nd data for bulk samples of Y-86032 are shown as light (yellow) circles, whereas those in mineral separates are shown as dark (red) squares. REE abundance patterns calculated from data presented by Karouji et al. (2004) for ,131 DG, 34 IM, and 36 IM lie within the shaded band. REE abundances for ,28 LG were provided by Y. Karouji (pers. comm.). Note that pyroxene separates from both ,28 LG and ,44 DG show the characteristic LREE depletion of pyroxene. Nd abundances for ,44 Plag and ,44 Px2 are nearly identical. Analysis of the ,28 Plag sample failed. (For interpretation of the references to color in this figure legend, the reader is referred to the web version of this paper.)

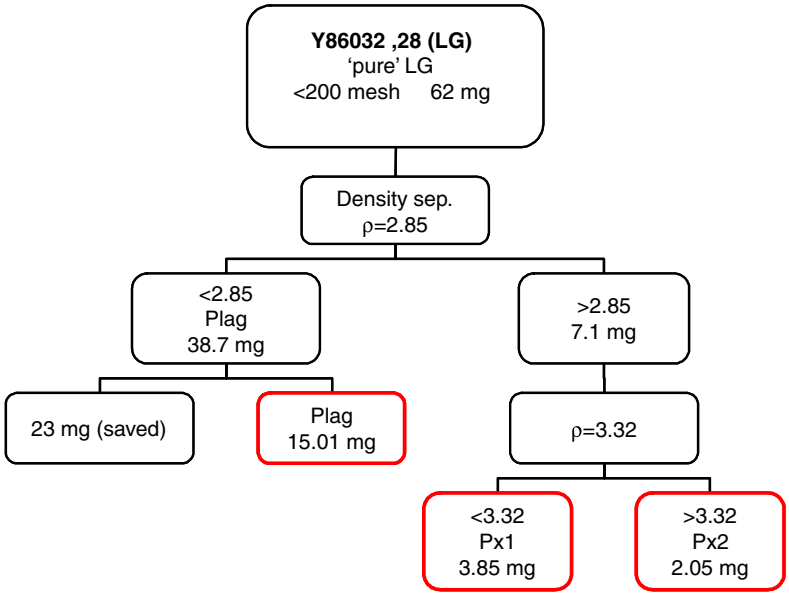


Fig. 6. Mineral separation scheme for light gray, feldspathic sample ,28 LG. Note that ,28 Px2, the purest pyroxene fraction, constituted ~5% by mass of the total processed through separation. This amount compares favorably to the modal abundance of large pyroxene grains in the sample.

*5.1.2. Sm–Nd isotopic data*

Fig. 8 shows that the Sm–Nd isotopic data (Table 4) yield a precise isochron age $T = 4.43 \pm 0.03$ Ga for combined data from LG ,28 and DG ,44. We have combined the data for these two lithologies because they are not distinct isotopically. Nevertheless, the isochron is primarily for ,28. It is anchored by the ,28 whole rock data at the lowest $^{147}Sm/^{144}Nd$ ratio, and by ,28 Px2 at the highest $^{147}Sm/^{144}Nd$ ratio. We attribute the coincidence of the data for ,28 whole rock and the ,44 plagioclase separate to the fact that the bulk composition of the LG-lithology is very anorthositic as shown by its low Fe content, the lowest among the LG, DG, and IM lithologies. The somewhat higher $^{147}Sm/^{144}Nd$ ratio of bulk ,44 DG shows that this sample contained a greater abundance of mafic minerals. Pyroxene analyses show two pyroxene populations at relatively low and relatively high Fe abundances, respectively, suggesting that two different anorthositic rock types contributed to the protolith of the LG-lithology. The Nd isotopic data suggest the two rock types were cogenetic.

*5.2. Rb–Sr isotopic data*

Rb–Sr data for Y-86032 (Table 5) show that ,28 plag, 28 LG, 28 Px1, and ,133 have low $^{87}Rb/^{86}Sr$ ratios and $^{87}Sr/^{86}Sr$ similar to those of Apollo 16 ferroan anorthosites

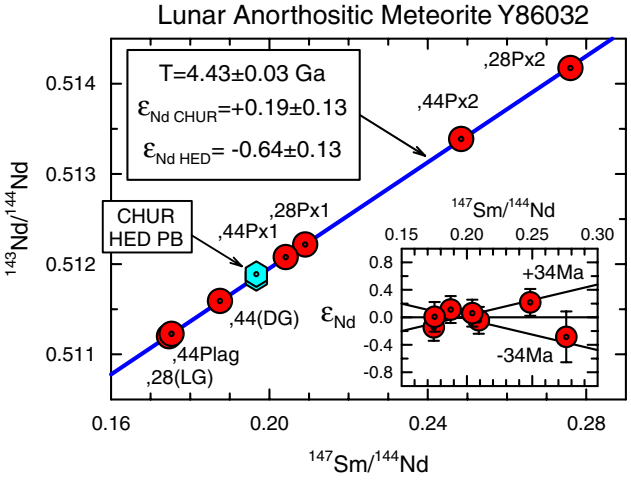


Fig. 8. Sm–Nd isochron for Y-86032,28LG and Y-86032,44DG (combined). As expected, the "Px 2" analyses of both samples plot at comparatively high $^{147}Sm/^{144}Nd$ ratios. Separated plagioclase from ,44DG and ,28LG plot at the lowest $^{147}Sm/^{144}Nd$ ratios. The data for all analyses are colinear within the error limits of ~0.3 $\varepsilon$-units suggesting that the analysed minerals came either from a single lithic precursor, or more likely, from cogenetic lithologies. Thus, we interpret the isochron age, $4.43 \pm 0.03$ Ga, as the age of crystallization of a primary crustal lithology or, possibly, a range of cogenetic lithologies. The initial $\varepsilon_{Nd}$ value of Y-86032 is slightly positive relative to CHUR (Jacobsen and Wasserburg, 1984), but is distinctly negative relative to initial $\varepsilon_{Nd}$ in eucritic meteorites (Nyquist et al., 2004). Thus, these samples of the lunar highlands crust could have crystallized from a feldspar-rich lunar magma ocean evolved from "chondritic" relative REE abundances as determined from eucrites.

like 60025 (Fig. 9). With the exception of ,28 Px1, the samples with the lowest $^{87}Rb/^{86}Sr$ are plagioclase separates, as is expected. Plagioclases from several Apollo 16 FAN samples form an apparently isochronous relationship with the 60025 and Y-86032 plagioclases. An isochron fitted to the Apollo 16 FAN plagioclase data gives an apparent age of $4.62 \pm 0.89$ Ga and initial $^{87}Sr/^{86}Sr = 0.699066 \pm 43$, where the $2\sigma$ uncertainty refers to the last digits. Both samples of ,133, that is, ,133 plag and ,133 Px, fall on the Apollo 16 FAN isochron. Although the isochron age is too imprecisely defined to give a useful independent estimate of the time of crystallization of these plagioclases, it nevertheless is consistent with the ~4.4 Ga Sm–Nd ages of 60025 and Y-86032, as well as the Ar–Ar age of Y-86032,116 presented below. Among the Y-86032 subsamples, 28 Px2, 44 Px2, 44 Px1, and the impact melt samples fall off the isochron. These subsamples have been open Rb–Sr systems in the interval after ~4.4 Ga. The subsamples that plot above the isochron show the effect of Rb loss and/or Sr gain during one or more secondary events. We attribute this either to loss of volatile Rb in one or more lunar impact events, weathering in the Antarctic environment, or possibly to enhanced processing blanks for small mg-sized samples. The analysis of the 21-mg sample ,33 IM, is robust, however. Because no mixing end member that could explain the higher Rb/Sr ratio of the impact melt compared to the LG and GC lithologies has been identified, we tentatively attribute the approximately sixfold higher Rb/Sr ratio of ,33 IM relative to ,28 LG to partitioning of Rb into the melt during impact melting. If so, the tie-line between ,33 IM and ,28 Plag giving an apparent age of $4.00 \pm 0.17$ Ga is an upper limit to the time of the melting event.

The observed range in $^{87}Rb/^{86}Sr$ ratios among the Y-86032 lithologies is small, and with the exception of the ,28 Px 2 analysis does not allow meaningful Rb–Sr ages to be independently calculated. Table 5 lists the Ar–Ar ages found for the various lithologies together with the calculated initial $(^{87}Sr/^{86}Sr)_I$ ratios. In general, these values are upper limits to initial $^{87}Sr/^{86}Sr$ present at crystallization in the dominant rock types contained in the breccia. Measured $^{87}Sr/^{86}Sr$ for ,43 DG is significantly higher than for ,44 DG WR and marginally higher than for the impact melt samples ,30 and ,33. Unfortunately, the Rb analysis for ,43 DG failed, but the $^{87}Sr/^{86}Sr$ values of the three samples ,30 IM, ,33 IM and ,43 DG are the highest among the analysed samples implying the greatest input of Rb- and other trace-element-rich material to these regolith samples. Thus, they apparently contain the most mature regolith component, a conclusion consistent with the relatively high neutron fluences they experienced (Fig. 5). The three samples ,37 IM, 44 DG, and 116 matrix, have lower measured $^{87}Sr/^{86}Sr$ implying a smaller input of Rb- and other trace-element-rich material, and thus a less mature regolith component. However, in general, the measured $^{87}Sr/^{86}Sr$ for all of the samples are low in comparison to those of known lunar rock types with the exception of ferroan anorthosites.

Table 4
The Sm–Nd analytical results for lunar meteorite Y-86032

| Sample | wt. (mg) | Sm (ppm) | Nd (ppm) | $^{147}Sm/^{144}Nd$[b] | $^{143}Nd/^{144}Nd$[b,c] | $T_{Ar-Ar}$ (Ga) | $\varepsilon_{Nd\ CHUR}$[e] | $\varepsilon_{Nd\ HED}$[f] |
|---|---|---|---|---|---|---|---|---|
| Y-86032,116 GC | | | | | | | | |
| WR[a] | 16.3 | 0.228 | 0.7993 | 0.17250 ± 27 | 0.511094 ± 14 | 4.38 ± 0.05 | −0.98 ± 0.32 | −1.81 ± 0.32 |
| Y-86032,116 matrix | | | | | | | | |
| WR | 18.5 | 0.436 | 1.57 | 0.16801 ± 17 | 0.511188 ± 10 | | | |
| Ames Nd standard : | | | | | | | | |
| $Nd^+$ | (7 analyses 12/95) : | | | | 0.511105 ± 14[d] | | | |
| $NdO^+$ | (4 analyses 12/95) : | | | | 0.511087 ± 26 | | | |
| Y-86032,28 LG (light-gray lith.) | | | | | | | | |
| WR | 20.7 | 0.34 | 1.177 | 0.17464 ± 23 | 0.511200 ± 10 | 4.10 ± 0.02 | −0.94 ± 0.23 | −1.77 ± 0.23 |
| Plag | 15.01 | — | — | | | | | |
| Px1 | 3.85 | 0.929 | 2.688 | 0.20903 ± 43 | 0.512217 ± 10 | | | |
| Px2 | 2.05 | 1.398 | 3.064 | 0.27601 ± 71 | 0.514174 ± 19 | | | |
| Y-86032,33 IM (impact melt) | | | | | | | | |
| WR | 21.4 | 0.5733 | 1.901 | 0.18236 ± 20 | 0.511376 ± 10 | 3.80 ± 0.10 | −2.20 ± 0.22 | −3.0 ± 0.22 |
| Y-86032,44 (dark-gray lith.) | | | | | | | | |
| WR | 23.25 | 0.6566 | 2.118 | 0.18750 ± 20 | 0.511592 ± 10 | 3.80 ± 0.10 | −0.46 ± 0.22 | −1.29 ± 0.22 |
| Plag | 14.3 | 0.4886 | 1.686 | 0.17527 ± 20 | 0.511227 ± 11 | | | |
| Px1 | 4.55 | 0.867 | 2.569 | 0.20412 ± 26 | 0.512078 ± 10 | | | |
| Px2 | 1.3 | 0.714 | 1.738 | 0.24840 ± 91 | 0.513388 ± 10 | | | |
| Ames Nd standard : | | | | | | | | |
| $NdO^+$ | (12 analyses 5/04) : | | | | 0.511099 ± 19[d] | | | |
| $NdO^+$ | (12 analyses 5/04) : | | | | 0.511121 ± 16[d] | | | |
| $NdO^+$ | (9 analyses 5/04) : | | | | 0.511122 ± 11[d] | | | |

[a] WR, whole rock; Plag, plagioclase; Px1, pyroxene + plagioclase; Px2, pyroxene.
[b] Uncertainties correspond to last figures and represent $\pm 2\sigma_m$ error limits.
[c] Normalized to $^{146}Nd/^{144}Nd = 0.724140$ and adjusted to $^{143}Nd/^{144}Nd = 0.511138$ for the Ames Nd standard (Wasserburg et al., 1981).
[d] Uncertainties correspond to last figures and represent $\pm 2\sigma_p$ error limits.
[e] Calculated at the Ar–Ar age for interlaboratory-adjusted $^{143}Nd/^{144}Nd = 0.505883$ and $^{147}Sm/^{144}Nd = 0.1967$ for CHUR at 4.567 Ga.
[f] Calculated at the Ar–Ar age for $^{143}Nd/^{144}Nd = 0.505926$ and $^{147}Sm/^{144}Nd = 0.1967$ for the HEDPB at 4.567 Ga.

Table 5
The Rb–Sr analytical results for lunar meteorite Y-86032

| Sample | wt. (mg) | Rb(ppm) | Sr(ppm) | $^{87}Rb/^{86}Sr$[b] | $^{87}Sr/^{86}Sr$[b,c] | $T_{Ar-Ar}$ (Ga) | $(^{87}Sr/^{86}Sr)_i$ |
|---|---|---|---|---|---|---|---|
| Y-86032,116 GC | 16.3 | 0.1170 | 159.8 | 0.00211 ± 2 | 0.699213 ± 20 | 4.40 ± 0.05 | 0.699079 ± 20 |
| Y-86032,116 matrix | 18.5 | 0.2890 | 157.4 | 0.00532 ± 3 | 0.699429 ± 11 | 3.8 ± 0.1 | 0.699138 ± 14 |
| Y-86032,28 LG | | | | | | | |
| WR[a] | 20.7 | 0.0747 | 178.9 | 0.00121 ± 2 | 0.699135 ± 10 | 4.10 ± 0.02 | 0.699063 ± 10 |
| Plag | 15.01 | 0.0901 | 238.1 | 0.00109 ± 2 | 0.699120 ± 10 | | |
| Px1 | 3.85 | 0.0624 | 126.6 | 0.00143 ± 3 | 0.699149 ± 10 | | |
| Px2 | 2.05 | 0.0278 | 15.69 | 0.00513 ± 46 | 0.699257 ± 12 | | |
| Y-86032,33 IM | 21.4 | 0.3800 | 154.7 | 0.00711 ± 8 | 0.699475 ± 10 | 3.8 ± 0.10 | 0.699086 ± 15 |
| Y-86032,44 DG | | | | | | | |
| WR[a] | 23.25 | 0.2854 | 143.5 | 0.00576 ± 5 | 0.699460 ± 10 | 3.8 ± 0.10 | 0.699145 ± 14 |
| Plag | 14.3 | 0.2974 | 182.9 | 0.00471 ± 5 | 0.699380 ± 10 | | |
| Px1 | 4.55 | 0.2521 | 113.0 | 0.00646 ± 8 | 0.699534 ± 10 | | |
| Px2 | 1.3 | 0.0829 | 22.78 | 0.0105 ± 5 | 0.699883 ± 10 | | |
| Y-86032,133 W | | | | | | | |
| WR[a] | 24.25 | — | 164.9 | — | 0.699193 ± 10 | | |
| Plag | 38.45 | 0.0911 | 164.2 | 0.00161 ± 1 | 0.699148 ± 13 | 4.25 ± 0.03 | 0.699049 ± 14 |
| Px | 0.8 | 0.1410 | 144.5 | 0.00282 ± 13 | 0.699252 ± 13 | | |
| Y-86032,37 IM | 20.7 | 0.2960 | 160.6 | 0.00534 ± 5 | 0.699396 ± 10 | 3.8 ± 0.1 | 0.699104 ± 14 |
| Y-86032,30 IM | 19.1 | 0.3280 | 148.4 | 0.00639 ± 6 | 0.699475 ± 11 | 3.8 ± 0.1 | 0.699125 ± 15 |
| Y-86032,43 DG | 19.55 | | 150.1 | | 0.699485 ± 10 | 3.8 ± 0.1 | |

[a] WR, whole rock.
[b] Uncertainties correspond to last figures and represent $\pm 2\sigma_m$ error limits.
[c] Normalized to $^{88}Sr/^{86}Sr = 8.37521$ and adjusted to $^{87}Sr/^{86}Sr = 0.710250$ for the NBS 987 Sr standard (Nyquist et al., 1990).

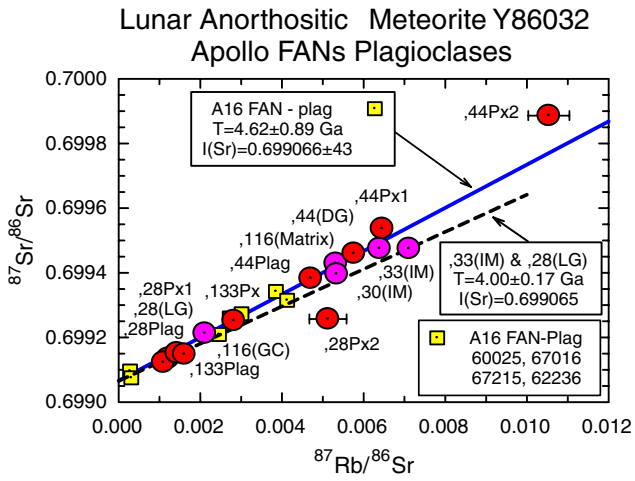


Fig. 9. Rb–Sr data for Y-86032 subsamples in comparison to those for some Apollo 16 FANs. A least-squares fit to data for the FANs gives a whole rock age of $4.62 \pm 0.89$ Ga and initial $^{87}Sr/^{86}Sr$ $(I(Sr)) = 0.699066 \pm 43$. A tie-line through LG ,28 bulk rock and the IM ,33 impact melt gives an apparent age of $4.00 \pm 0.17$ Ga, an estimate of the time the impact melt formed. The data for the pyroxene samples appear to be disturbed. We attribute this either to weathering in the Antarctic environment, or possibly to enhanced processing blanks for these mg-sized samples. Thus, we give no time significance to those data. The analysis of the 21-mg sample ,33 IM, however, is robust (Table 3). Thus, its displacement from the alignment of other robust analyses is significant. We tentatively attribute the higher Rb/Sr ratio of ,33 IM to partitioning of Rb into the melt during impact melting. In this case, the tie-line between it and ,28 Plag giving an apparent age of $4.00 \pm 0.17$ Ga is a probable upper bound to the time of the melting event.

### 5.3. Ar–Ar ages of distinct Y-86032 lithologies

#### 5.3.1. Experimental

Five different samples of Y-86032, along with several samples of the NL-25 hornblende age monitor, were irradiated with fast neutrons at the University of Missouri Research Reactor (MURR). The irradiation constant, $J$, for, 116 GC was $0.0312 \pm 0.003$. This irradiation used BN to shield thermal neutrons. The irradiation constants for a separate irradiation of samples ,28 (LG-lithology) and ,33 (IM-lithology) were $0.0214 \pm 0.0001$ and $0.0215 \pm 0.0015$, respectively. Two additional irradiations of sample ,30 (DG-lithology) and sample ,133 (a light feldspathic clast) gave $J$ values of $0.02051 \pm 0.00003$ and $0.01990 \pm 0.00007$, respectively. Each sample was degassed by stepwise heating, and the argon isotopic composition measured on a VG-3600 mass spectrometer. Uncertainties reported for individual ages include errors in measuring the $^{39}Ar/^{40}Ar$ ratio and uncertainties in blank and reactor corrections. Because reactor corrections are large for samples with high Ca/K ratios, we went to considerable effort to define these corrections precisely for our MURR irradiations. This included determining more precisely the half-life of $^{37}Ar$, which is the measured parameter used to make such corrections, and documenting effects of fuel cycle on correction factors. These data are presented and discussed in the Appendix A. Other experimental details are given in Bogard et al. (2000b).

#### 5.3.2. Y-86032,116

The Ar–Ar age spectrum for a 17.1 mg subsample of Y-86032,116GC is presented in Fig. 10. Reactor corrections to $^{39}Ar$ for most extractions were ~40%. The measured [K] of 74 ppm and [Ca] of 12.2% are consistent with nearly pure anorthite. The K/Ca ratio is constant at $\sim 6 \times 10^{-4}$ throughout the release, and most of the Ar was released at relatively high temperatures of 1100–1400 °C. The first four extractions (0–15% $^{39}Ar$ release) show decreasing $^{36}Ar/^{37}Ar$ and $^{36}Ar/^{38}Ar$ ratios and Ar–Ar ages, consistent with release of adsorbed terrestrial Ar. Intermediate temperature extractions show increasing Ar–Ar ages indicative of prior $^{40}Ar$ diffusion loss. No age plateau is attained. However, the 1400 °C extraction released 28% of the total $^{39}Ar$ and gives an age of $4.414 \pm 0.035$ Ga (where the error includes the uncertainty in irradiation constant, $J$). Because of the possibility of $^{40}Ar$ diffusion loss from even the 1400 °C extraction, this is a lower limit to the Ar retention age.

We must consider corrections to this age necessitated by $^{40}Ar$ implanted from the lunar atmosphere along with solar wind $^{36}Ar$ and $^{38}Ar$. For eight extractions (releasing 15.5–99.5% of the $^{39}Ar$), the measured $^{38}Ar/^{36}Ar$ ratios vary a factor of two and the $^{37}Ar/^{36}Ar$ ratios vary a factor of three. This variability indicates a mixture of two components— trapped solar wind Ar and a nuclear component consisting of $^{38}Ar$ and $^{36}Ar$ produced from Ca by cosmic rays plus $^{37}Ar$ produced from Ca in the reactor. A plot (not shown) of $^{38}Ar/^{37}Ar$ versus $^{36}Ar/^{37}Ar$ for these eight extractions is linear ($R^2 = 0.9935$), which indicates the solar and nuclear components have essentially constant Ar isotopic compositions. This plot gives a trapped $^{38}Ar/^{36}Ar$ of $0.1925 \pm 0.0064$ and a slope of $0.00152 \pm 0.00002$. Adopting cosmogenic $^{36}Ar/^{38}Ar = 0.67$, this slope indicates a constant nuclear $^{37}Ar/^{36}Ar$ component of $661 \pm 8$ across these eight extractions. From the nuclear $^{37}Ar/^{36}Ar$ ratio,

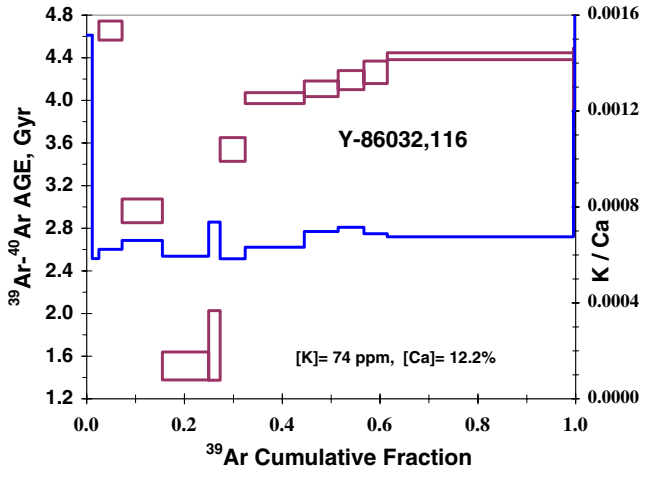


Fig. 10. $^{39}Ar$–$^{40}Ar$ ages (rectangles, left scale) and K/Ca ratios (stepped line, right scale) versus cumulative release of $^{39}Ar$ for stepwise temperature release of Y-86032,116GC. Width of the age rectangles indicate analytical age uncertainties, not considering the uncertainty in $J$.

we calculated the cosmogenic $^{36}Ar$ for each extraction. The solar wind $^{36}Ar$ concentration for each extraction was then determined by subtracting $^{36}Ar_{cos}$ from the measured $^{36}Ar$ (see Garrison et al. (2000) for details).

Studies of many Apollo samples have shown that solar wind $^{36}Ar$ is always accompanied by an $^{40}Ar$ component implanted from the lunar atmosphere, where the trapped $^{40}Ar/^{36}Ar$ ratio is typically ~0.3–1.0 for material exposed at the lunar surface within the past ~1 Ga. Lunar samples exposed to the solar wind at much earlier times contain significantly higher trapped $^{40}Ar/^{36}Ar$ ratios, but the exact change in this ratio back in time is not known. McKay et al. (1986) suggested that the $^{40}Ar/^{36}Ar$ ratio increased inversely with the abundance of $^{40}K$ to values of ~10 at 4.0 Ga ago. Using a different data set, Eugster et al. (2001) suggested a slightly different change in trapped $^{40}Ar/^{36}Ar$ with time. These two data sets predict similar $^{40}Ar/^{36}Ar$ back to ~3.8 Ga ago, but for earlier times the trend given by Eugster et al. (2001) predicts considerably larger ratios, possibly 15 or more for ages >4 Ga. Eugster et al. (1989) derived a trapped $^{40}Ar/^{36}Ar$ ratio of $12.1 \pm 3.0$ from several analyses of Y-86032. The $^{40}Ar/^{36}Ar$ intercept of the trend defined by these data is strongly dependent on a single whole rock analysis. Below we present evidence for a trapped $^{40}Ar/^{36}Ar$ ratio of ~15 in one of the samples we analyzed. Thus, for Y-86032 samples discussed here, we give the Ar–Ar age corrected for trapped $^{40}Ar/^{36}Ar$ ratios of 5, 10, and 15. Applying these assumed trapped $^{40}Ar/^{36}Ar$ corrections to the 1400 °C extraction of Y-86032,116 gives corrected ages of $4.397 \pm 0.035$, $4.380 \pm 0.035$, and $4.363 \pm 0.035$ Ga, respectively, compared to the uncorrected age of 4.414 Ga. Thus, the Ar–Ar age of the 1400 °C extraction of Y-86032,116 likely lies in the range 4.36–$4.40 \pm 0.035$ Ga. Because the 1400 °C extraction also may have lost some of its $^{40}Ar$ by diffusion, it is possible that the original Ar–Ar age of this clast is identical to the $4.43 \pm 0.04$ Ga Sm–Nd isochron age presented above for Y-86032 lithologies.

### 5.3.3. Y-86032,133

The Ar–Ar age spectrum for a 30 mg sample of ,133 is presented in Fig. 11. This clast was taken from original parent sample ,20 (Takeda et al., 1989) and is thought to be similar to clast sample ,116 GC. The first three extractions (350–500°C) released 57% of the total $^{39}Ar$ from a phase with a K/Ca ratio two orders of magnitude higher than lunar anorthite, and this release was accompanied by significant amounts of terrestrial $^{40}Ar$. We attribute this Ar release to terrestrial weathering products on grain surfaces, in an amount not observed in the other samples analyzed, and we discount these data. To better show detail, Fig. 11 gives only the age spectrum above 50% $^{39}Ar$ release. Between 57% and 68% $^{39}Ar$ release the age spectrum resembles those of samples ,116 GC and ,28 LG in that the age decreases as terrestrial $^{40}Ar$ is degassed, then rapidly increases. Five extractions (68–81% $^{39}Ar$ release) suggest a plateau age of $3.87 \pm 0.03$ Ga. At higher extraction temperatures the age increases to a maximum value of $4.28 \pm 0.03$ Ga (at 1400 °C). The $^{36}Ar/^{37}Ar$ and $^{36}Ar/^{38}Ar$ ratios are approximately constant for extractions releasing >68% of the $^{39}Ar$, but the average $^{36}Ar/^{38}Ar$ ratio of 0.92 is larger than the expected cosmogenic ratio of ~0.66 and indicates the release of small amounts of solar wind Ar. Thus, we applied a correction to $^{40}Ar$ by assuming trapped $^{40}Ar/^{36}Ar = 15$, trapped $^{36}Ar/^{38}Ar = 5.4$, and cosmogenic $^{36}Ar/^{38}Ar = 0.66$. This correction decreased the plateau age to 3.81 Ga and the oldest age to 4.23 Ga. The age spectrum above ~68% $^{39}Ar$ release indicates a classical $^{40}Ar$ diffusion loss profile and suggests sample ,133 had an original age of >4.23 Ga and was very strongly degassed ~3.81 Ga ago, possibly by the same event that degassed sample ,30 (discussed below).

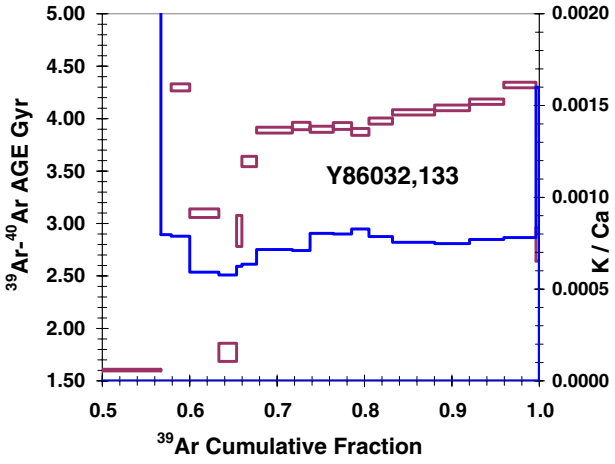


Fig. 11. $^{39}Ar$–$^{40}Ar$ ages (rectangles, left scale) and K/Ca ratios (stepped line, right scale) versus cumulative release of $^{39}Ar$ for stepwise temperature release of Y-86032,133.

### 5.3.4. Y-86032,28

The Ar–Ar age spectrum for a 27.3 mg subsample of the LG-lithology (*cf.* Fig. 1) is presented in Fig. 12. Reactor corrections to $^{39}Ar$ for most extractions were ~25%. The measured [K] and [Ca] are 145 ppm and 11.0%, respectively. The K/Ca ratio of the Ar–Ar sample was relatively constant at ~0.002 and most of the Ar was released at temperatures of 1150–1400 °C. Higher K/Ca ratios in the first two extractions suggest addition of K to grain surfaces, possibly during Antarctic weathering. The first few extractions (~0–10% $^{39}Ar$ release) show decreasing $^{36}Ar/^{37}Ar$, $^{36}Ar/^{38}Ar$, K/Ca ratios, and Ar–Ar ages, consistent with release of adsorbed terrestrial Ar. A steady increase in age across 17–39% $^{39}Ar$ release suggests some $^{40}Ar$ diffusion loss. However, eight extractions releasing ~39–100% of the $^{39}Ar$ show an age plateau with an average value of $4.108 \pm 0.017$ Ga (including the uncertainty in *J*).

There is only minimal evidence for trapped solar wind $^{36}Ar$ in sample ,28 LG, and this is consistent with the short regolith-residence time indicated by its low thermal

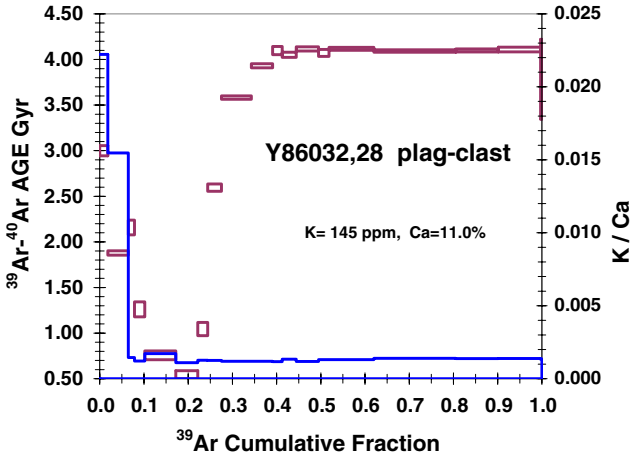


Fig. 12. $^{39}$Ar–$^{40}$Ar ages (rectangles, left scale) and K/Ca ratios (stepped line, right scale) versus cumulative release of $^{39}$Ar for stepwise temperature release of Y-86032,28 LG.

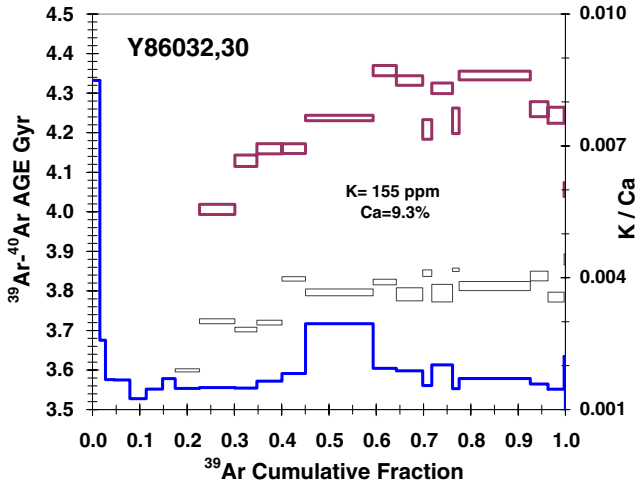


Fig. 13. $^{39}$Ar–$^{40}$Ar ages (rectangles, left scale) and K/Ca ratios (stepped line, right scale) versus cumulative release of $^{39}$Ar for stepwise temperature release of Y-86032,30 DG. Two age spectra are shown. The older age spectrum (bold rectangles) has no correction applied for trapped $^{40}$Ar. The lower age spectrum (light rectangles) is the result of correcting for trapped $^{40}$Ar by assuming trapped $^{40}$Ar/$^{36}$Ar = 15.

neutron fluence (Fig. 5). Above ~8% $^{39}$Ar release the measured $^{36}$Ar/$^{38}$Ar ratio is relatively constant at approximately the expected cosmogenic value. An exception is the 1220 °C extraction, where increases in both the $^{36}$Ar/$^{38}$Ar and $^{36}$Ar/$^{37}$Ar ratios suggest release of trapped $^{36}$Ar. Among those eight extractions that define the age plateau, we adopted the highest measured $^{37}$Ar/$^{36}$Ar ratio to represent a pure nuclear component and applied corrections for trapped $^{36}$Ar to the remaining extractions (see above). Assuming trapped $^{40}$Ar/$^{36}$Ar ratios of 5, 10, and 15, the corrected plateau ages become $4.104 \pm 0.017$, $4.099 \pm 0.017$, and $4.095 \pm 0.017$ Ga, respectively. Thus, we adopt an age of $4.10 \pm 0.02$ Ga for Y-86032,28. The age spectrum in Fig. 12 shows the age corrected for trapped $^{40}$Ar/$^{36}$Ar = 10.

### 5.3.5. Y-86032,30

The Ar–Ar age spectrum for this sample of the DG lithology located adjacent to the impact melt vein (Fig. 1) is presented in Fig. 13. Our allocation of this lithology contained both light (~LG and/or ~W) and dark (~IM) material. The sample used for Ar–Ar was enriched in lighter material, whereas that used for Sm-isotopic measurements was enriched in impact melt. The first five extractions (0–11% of the $^{39}$Ar) released adsorbed terrestrial Ar, and an isochron plot of these data ($R^2 = 0.995$) gives an $^{40}$Ar/$^{36}$Ar intercept close to the terrestrial value and an age of ~0.97 Ga. We ascribe no time significance to this "age", because it is associated with weathered phases. All extractions up to ~40% of the $^{39}$Ar release indicate prior diffusion loss of radiogenic $^{40}$Ar. Above 40% $^{39}$Ar release (1150–1400 °C) the Ar–Ar age shows apparently random scatter over ~4.23–4.35 Ga. Sample ,30 also released significant quantities of trapped solar wind $^{36}$Ar with a nearly constant $^{36}$Ar/$^{38}$Ar ratio of ~2.5. Thus, corrections to individual Ar ages are required for lunar atmosphere $^{40}$Ar. Fig. 13 shows the Ar–Ar ages assuming trapped $^{40}$Ar/$^{36}$Ar ratios of 0 and 15. The maximum $^{40}$Ar correction produces ages (for >45% $^{39}$Ar release) ranging between 3.79 and 3.85 Ga.

An isochron plot (Fig. 14) of $^{40}$Ar/$^{36}$Ar versus $^{39}$Ar/$^{36}$Ar for those ,30 DG extractions above 45% $^{39}$Ar release supports the above age interpretation. Cosmogenic $^{36}$Ar averages ~10% of the total $^{36}$Ar. This component was subtracted, and only the trapped solar wind $^{36}$Ar concentrations were used to construct this plot. The linearity of the isochron indicates these extractions have a constant Ar age of $3.80 \pm 0.07$ Ga and a single trapped $^{40}$Ar/$^{36}$Ar

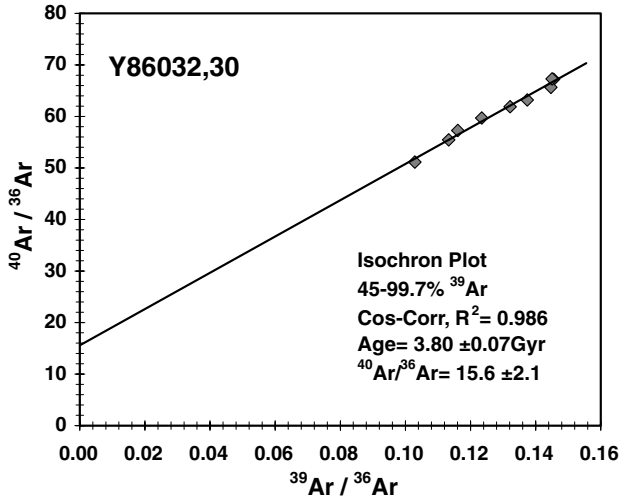


Fig. 14. Isochron plot of $^{40}$Ar/$^{36}$Ar versus $^{39}$Ar/$^{36}$Ar for eight extractions of Y-86032,30 releasing 45–99.7% of the $^{39}$Ar. Cosmogenic $^{36}$Ar, amounting to ~10% of the total, has been subtracted from each datum to yield only the trapped solar wind $^{36}$Ar. The isochron gives an Ar age of $3.80 \pm 0.07$ Ga and a $^{40}$Ar/$^{36}$Ar intercept of $15.6 \pm 2.1$.

ratio of $15.6 \pm 2.1$. This age is in agreement with the 3.81 Ga age derived above for sample ,133, for which the trapped Ar corrections were much less. Thus, we suggest an age of $3.8 \pm 0.1$ Ga measures the time of a significant thermal event in the history of Y-86032.

### 5.3.6. Y-86032,33

The Ar–Ar age spectrum for a 29.5 mg subsample of impact melt is presented in Fig. 15. The measured [K] and [Ca] are 210 ppm and 11.8%, respectively, and the K/Ca ratio is relatively constant at ~0.0017 across much of the $^{39}$Ar release. Most of the $^{39}$Ar was released at temperatures of 1150–1400 °C, indicating that the K is hosted in retentive phases. The first seven extractions (0–9% $^{39}$Ar release) show significantly decreasing K/Ca and $^{36}$Ar/$^{37}$Ar ratios and Ar–Ar ages, which are indicative of weathering effects. Over ~20–100% $^{39}$Ar release the Ar–Ar age shows apparently random scatter. In this range, the maximum and minimum ages (uncorrected for trapped $^{40}$Ar) are 4.37 and 4.17 Ga, which is similar to the range shown by uncorrected ages for ,30 DG. Over 20–100% $^{39}$Ar release, the $^{36}$Ar/$^{38}$Ar ratio is relatively constant at $2.62 \pm 0.08$ and indicates the release of significant amounts of solar wind $^{36}$Ar. If we apply a correction for trapped $^{40}$Ar assuming $^{40}$Ar/$^{36}$Ar = 15, the maximum and minimum ages decrease to 3.88 and 3.70 Ga (Fig. 15). However, even with this correction for lunar atmospheric $^{40}$Ar, the individual ages for ,33 IM still scatter by an amount larger than the uncertainties in individual ages. An isochron plot (not shown) of $^{40}$Ar/$^{36}$Ar versus $^{39}$Ar/$^{36}$Ar shows considerable scatter ($R^2 = 0.44$), and is much less well defined compared to the ,30 DG isochron (Fig. 14). We suggest that the residual scatter in individual Ar–Ar ages of ,33 IM may be produced by the melt having incorporated materials of old and possibly differing ages, which were not totally degassed of their radiogenic $^{40}$Ar at the time of melt injection.

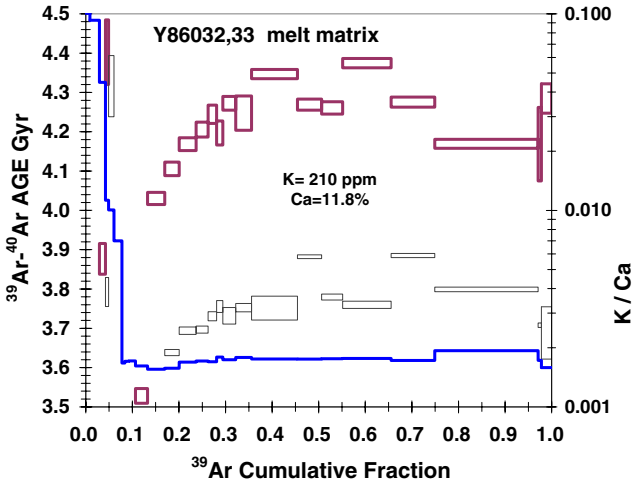


Fig. 15. $^{39}$Ar–$^{40}$Ar ages (rectangles, left scale) and K/Ca ratios (stepped line, right scale) versus cumulative release of $^{39}$Ar for stepwise temperature release of Y-86032,33 IM. Two age spectra are shown. The older age spectrum (bold rectangles) has no correction applied for trapped $^{40}$Ar. The lower age spectrum (light rectangles) is the result of correcting for trapped $^{40}$Ar by assuming trapped $^{40}$Ar/$^{36}$Ar = 15.

The absolute earliest possible time of formation of the Y-86032 breccia would be ~3.8–4.1 Ga, as given by the ages of clasts ,133 and ,28 LG, corrected for implanted $^{40}$Ar. However, considering reasonable corrections for trapped $^{40}$Ar, the Ar–Ar ages for sample ,30 DG and likely also melt sample ,33 IM are $3.8 \pm 0.1$ Ga. We suggest this is the most likely time of formation of the Y-86032 breccia and impact melt within it.

Interestingly, the [Ca] content of this impact melt (11.8%) is nearly as high as that for ,116 GC (12.2%), suggesting that the protolith for the impact melt was dominantly anorthositic. Larger samples of impact melt analysed by INAA at Tokyo Metropolitan University (Karouji et al., 2004) had slightly lower average [Ca] = 11.0% and variable [K] from 107 to 367 ppm. The average [K] = 237 ppm is similar to [K] = 210 ppm for the Ar–Ar subsample. At the lower end of the [K] range, [K] = 107 ppm suggests that melts of very anorthositic composition remain incompletely homogenized within the IM-lithology at the scale of the samples used for INAA analysis.

## 6. Discussion

### 6.1. Chronology of Y-86032 and the age of its protolith

The Sm–Nd age of $4.43 \pm 0.03$ Ga for minerals from ,28 LG and ,44 DG indicates early formation of the protolith of Y-86032. Further, the lower limit of 4.35–4.41 Ga for the Ar–Ar age of ,116 GC may still be influenced by $^{40}$Ar diffusive loss and the Ar–Ar age may be consistent with the Sm–Nd age. The same may be said of the maximum age of $4.23 \pm 0.03$ Ga found for sample ,133. As discussed earlier in the paper, remnants of different rock types are present in the breccia, but the protolith was dominantly feldspathic. The modal mineral abundances in LG resemble those in FANs, but the detailed mineral chemistry differs from that of FANs (Yamaguchi et al., 2004, 2005). In particular, plagioclase compositions in LG peak near An ~93 with a secondary peak at An ~88.5 (Fig. 3a). Plagioclase of An ~93 is more sodic than that of typical FANs, and more typical of Mg-suite rocks like norites. However, trivalent REE abundances in the LG lithology are only slightly enriched relative to those in FANs (Fig. 7), and nearly sixfold lower than in typical norites like 78235. Thus, the dominant lithology in LG has no direct analog among known lunar rock types, but will be referred to here as "An93 anorthsite". The higher An contents of ,116 GC are similar to those of FANs, although mg' in mafic minerals present in this lithology are generally higher. Moreover, as discussed later in the paper, the Nd-isotopic systematics of ,116 GC differ from those of FANs. Consequently, we refer to the dominant lithology present in this clast as "An97 anorthosite". A more complete description of these

lithologies awaits the detailed mineralogical and chemical interpretations planned for a subsequent paper.

The Sm–Nd age of ~4.43 Ga for the combined LG and DG lithologies and the Ar–Ar age for ,116 GC are similar to the crystallization ages of ferroan anorthosite 60025 (Carlson and Lugmair, 1988), and of ferroan noritic anorthosite clasts from breccias 67016 (Alibert et al., 1994) and 67215 (Norman et al., 2003), and slightly older than the Sm–Nd age of $4.29 \pm 0.06$ Ga of ferroan anorthosite 62236 (Borg et al., 1999). Although FANs are generally considered to be flotation products from the primordial lunar magma ocean (LMO), and thus to have formed earlier than Mg-suite rocks like the norites, some norites have similarly old radiometric ages. Carlson and Lugmair (1981) reported an ~4.34 Ga age for norite 78236, but noted that the Sm–Nd isotopic systematics bore evidence of post-crystallization isotopic disturbance. Nyquist et al. (1981) preferred an older age of $4.43 \pm 0.05$ Ga from their Sm–Nd study and argued that slow cooling in the lunar crust may have reset some of the other chronometers. Shih et al. (1993) found Sm–Nd ages of $4.47 \pm 0.07$ Ga for noritic clast 15445, 17, but a younger age of $4.28 \pm 0.03$ for noritic clast 15445, 247. Thus, the ages found here for probable farside lunar crustal lithologies are in agreement with those of crustal rocks of lunar nearside origin. Because the Y-86032 samples were breccias, both the Ar–Ar and Sm–Nd ages are lower limits to the emplacement age of the protolith, and thus to the formation age of the lunar crust at the place of origin of Y-86032. Because of the geochemical evidence already presented and isotopic data to be presented, we consider a farside origin to be highly likely. In the following we will refer to the farside(?) origin to Y-86032 to acknowledge some uncertainty in this conclusion, however.

A detailed comparison of the chronology of farside(?) and nearside crustal rocks based on this study is hampered by lack of complete correspondence between farside(?) and nearside crustal rock types. Using the An content of plagioclase as a guide, the $(4.36–4.40) \pm 0.035$ Ga age of ,116 GC is most appropriately compared to the ages of nearside FANs, and the $4.43 \pm 0.03$ age of the LG lithology probably is most appropriately compared to the ages of nearside norites. Note, however, that LG is significantly lower in the KREEP component characterizing the nearside Procellarum KREEP Terrain (PKT) than are norites. The younger Ar–Ar age of $4.10 \pm 0.02$ Ga for ,28 LG compared to nearside norites and anorthosites indicates thorough Ar outgassing prior to its lithification.

Incomplete Ar loss from some materials in the Y-86032 protolith following major impact events is clearly shown by the Ar–Ar age spectra for Y-86032,133. Also, total Ar loss was not achieved even during formation of the impact melt lithology, as shown by the Ar–Ar age spectra for Y-86032,30. Comparing to the results of earlier investigations, Kaneoka and Takaoka (1987) reported an Ar–Ar analysis of a mixed impact glass plus matrix sample of the paired meteorite Y-82192. Extractions up to 1300 °C gave uncertain ages of $\geqslant 5$ Ga, and the 1600 °C extraction, releasing most of the $^{39}Ar$, gave an age of $4.237 \pm 0.165$. Although the measured $^{36}Ar/^{38}Ar$ was 3.26 in the 1600 °C extraction, a correction for lunar atmosphere $^{40}Ar$ apparently was not applied. When we apply a correction assuming trapped $^{40}Ar/^{36}Ar = 15$, we calculate a corrected age of ~3.7 Ga. These results are in reasonable agreement with the more precise ages reported here.

When did the Y-86032 breccia form? The Ar–Ar data for sample ,30 DG suggests $3.8 \pm 0.1$ Ga ago, and the data for ,33 IM, as well as the corrected age for Y-82192, are consistent with this time. The time of significant degassing of clast sample ,133 at ~3.81 Ga also is consistent with this age. As noted above, a Rb–Sr tie line age for the impact melt ,33 IM and ,28 LG gives an age of $4.00 \pm 0.17$ Ga, which within errors is consistent with the Ar–Ar age, but which may also show partial resetting. The Ar–Ar ages of clasts ,116 GC and ,28 LG probably were set by impact heating events prior to breccia formation. The very flat plateau age of ,28 LG suggests that lithic components contributing to it were totally degassed of Ar during formation of the LG lithology, whereas the Ar–Ar ages of ,116 GC and sample ,133 were only partially reset. The Y-86032 components existed separately from one another during these earlier heating events. The final assembly of the breccia was coincident with injection of the impact melt. It appears this occurred during the time period of the hypothesized "lunar cataclysm" ~3.8–3.9 Ga ago (Tera et al., 1974; Ryder, 2002), but it also is clear that Y-86032 contains components lithified prior to the lunar cataclysm, at least as early as ~4.1 Ga ago, and possibly as early as ~4.38 Ga ago.

### 6.2. Cosmic ray exposure

We analyzed a 33 mg unirradiated sample of Y-86032,116GC for cosmogenic He, Ne and Ar. Cosmogenic concentrations were (in units of $10^{-8}$ $cm^3STP/g$): $^3He = 5.4$, $^{21}Ne = 0.53$, and $^{38}Ar = 2.2$. If we use the average chemical composition of Y-86032 reported in Table 2 and the 4-π, (space-exposure) elemental production rates given by Eugster and Michel (1995), we calculate cosmic ray exposure ages of $^3He = 3.1$ Ma, $^{21}Ne = 2.4$ Ma, and $^{38}Ar = 10.3$ Ma. The lower He and Ne ages probably represent diffusion loss from feldspar, which is commonly observed. Eugster et al. (1989) reported CRE ages for Y-86032 and paired meteorites Y-86192-3 to be ~10.6 Ma, assuming 4-π irradiation in space as small objects.

We can also estimate the concentration of $^{38}Ar_{cos}$ from each of our irradiated samples by assuming Ar is a mixture of cosmogenic and trapped components and by omitting apparent terrestrial Ar released at low temperatures. In the case of ,28 LG essentially all of the $^{38}Ar$ is cosmogenic. The concentration of $^{38}Ar$ in irradiated samples ,116 GC and ,28 LG are each $\sim 2.2 \times 10^{-8}$ $cm^3STP/g$, identical to $^{38}Ar_{cos}$ in the unirradiated sample of ,116 GC. Calculated $^{38}Ar_{cos}$ concentrations in ,33 IM and ,30 DG are higher at 5.0 and $3.4 \times 10^{-8}$ $cm^3STP/g$, respectively. Because of

larger relative concentrations of solar Ar in these two samples, their $^{38}Ar_{cos}$ concentrations are possibly more uncertain. However, it is reasonable to expect that the surface-irradiated material that contributed solar wind Ar to these samples also acquired larger amounts of $^{38}Ar_{cos}$. Thus, we conclude that the matrix phases of Y-86032 were exposed to cosmic rays near the lunar surface for at least a few Ma, whereas clasts ,28 LG and ,116 GC experienced very little pre-irradiation by cosmic rays on the lunar surface.

Eugster (1989) and Eugster et al. (1989) presented a detailed analysis of the exposure history of Y-86032/Y-82192/3 from cosmogenic noble gases and the radionuclides $^{10}$Be (half-life $1.5 \times 10^6$ years), $^{26}$Al ($7.05 \times 10^5$ years), and $^{53}$Mn ($3.7 \times 10^6$ years). Because the activities of the radionuclides were consistent with typical meteoritic values for 4π exposure in space, they favored a model in which the entire exposure of these paired meteorites to cosmic rays occurred in space. However, our data show that different Y-86032 lithologies experienced different total exposures to cosmic rays and secondary neutrons, and variable meteoritic contamination. Moreover, the presence of solar $^{36}$Ar in several samples shows that regolith exposure of some of the lithologies must have occurred $\geqslant$3.8 Ga ago. Thus, our data indicate an alternate irradiation model, similar to Model C of Eugster (1989, Fig. 5). That model requires an early irradiation of ~7 Ma near the lunar surface, followed by a long period during which the meteorites are shielded at depth from the cosmic radiation, followed by ejection into space ~7 Ma ago. Our preference for this scenario derives from consideration of a data set that is more extensive than the one available to Eugster et al. (1989).

Vogt et al. (1991) used data for a suite of radionuclides to deduce that Y-86032 experienced a $10 \pm 2$ Ma space exposure and essentially no lunar surface exposure, i.e., lunar exposure at >1000 g/cm$^2$ depth. Among the radionuclides they measured, only $^{10}$Be would be expected to retain any memory of lunar surface production, and only ~3% of any surface production on the Moon would persist after 8 Myr in space. In comparison, the analytical uncertainties in the measured $^{10}$Be concentrations were ~10%. Thus, the evidence given by Vogt et al. (1991) reveals little about the conditions of Y-86032 exposure on the Moon. The Sm isotopic data presented here are much more informative in that regard.

Our new data are consistent with a two-stage irradiation model. The relative neutron exposure of ,116 GC and ,28 LG suggest a second-stage, space exposure (4π irradiation of ~7–9 Ma), and those lithologies with a more extended regolith history suggest a first-stage, lunar surface exposure (2π irradiation) of up to ~16 Ma (calculated for the equivalent 4π exposure), if ,116 GC and ,28 LG were completely shielded prior to ejection into space. The relative $^{38}Ar_{cos}$ contents of ,116 GC and ,28 LG agree with such a scenario, although indicating slightly longer 4π and 2π exposure histories of ~10 and ~23 Ma (calculated for the equivalent 4π exposure), respectively.

The percentage error limits on the neutron fluences are large, precluding more detailed comparisons, but these cosmic-ray exposure indicators are qualitatively consistent with one another and with the relative Ir contents of the different lithologies, another indicator of regolith exposure. Since, for example, a variation in secondary neutron fluence of $10^{15}$ n/cm$^2$ is clearly detectable (*cf.* Fig. 5) the secondary neutron flux must have been reduced below $\sim 2.5 \times 10^{11}$ n/cm$^2$ Ma$^{-1}$ to effectively shield Y-86032 over ~4000 Ma. This is a factor of $\sim 1.5 \times 10^{-3}$, or $\sim e^{-6.5}$ below that in the Chico and Torino meteorites as discussed earlier in the paper. Assuming an exponential decay of the neutron flux with an e-folding length of ~250 g/cm$^2$ at depths below ~300 g/cm$^2$ (Armstrong and Alsmiller, 1971), a shielding depth of ~1675 g/cm$^2$ would be required. Lorenzetti et al. (2005) estimated 2π-shielding depths of >500 g/cm$^2$ for several lunar meteorites from cosmogenic $^{21}$Ne/$^{38}$Ar ratios, but their calculation is insensitive at high shielding depths. The shielding depth calculated here is equivalent to ~9 m for average lunar regolith of density ~1.8 g/cm$^3$, or ~5 m for coherent rock.

### 6.3. Megaregolith history of the Y-86032 lithologies

Fig. 16 summarizes the available textural, chemical, chronological, and surface irradiation information bearing on the megaregolith history of the Y-86032 lithologies. The parameters to be considered include: (1) The primary lithic components in the breccia; (2) The extra-lunar components, either direct (meteoritic components and solar wind), or indirect (products of nuclear interactions with galactic cosmic rays (GCR), or thermalized secondary neutrons); (3) The time interval over which these components were assembled; (4) Lithification events specific to a particular lithology; (5) The time of lithification of the Y-86032/Y-82192/3 parent breccia; (6) The time when the parent breccia was launched to earth.

As discussed above, two samples of the large, external clast shown in Fig. 1 of Takeda et al. (1989) were included in this investigation, and are identified as belonging to the "white clast" lithology. The primary rock type contributing to this lithology appears to have been the FAN-like An97 anorthosite, with only minor contributions from other rock types. The high temperature age plateau of ,116 GC provides an upper limit of <~4.36 Ga ago to the time of initial brecciation of this lithology. The maximum age of ~4.23 Ga for ,133 is plausibly a better estimate of the time of lithification of the large clast. Both samples indicate early formation of An 97 anorthosite. The Ar–Ar analysis of sample ,133 also suggests an event at 3.8 Ga ago, coincident with the time of final assembly of Y-86032 as recorded in the IM and DG lithologies.

Only a few primary components appear to have contributed to the LG lithology, with only two of them being volumetrically significant. The LG-lithology is likely to have been a pre-existing breccia of a single suite of igneous rocks prior to final lithification, because of the close proximity of

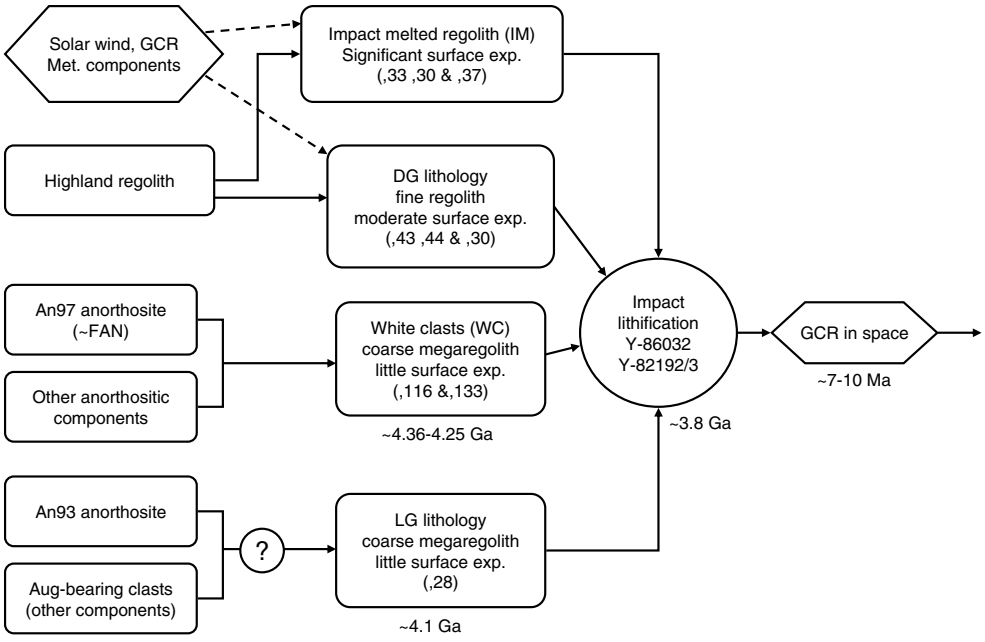


Fig. 16. The history of Y-86032/Y-82192/3 in the farside(?) megaregolith as deduced from this investigation. Primary components are represented at the left of the diagram, *in situ* lithic components in boxes, extra-lunar components (galactic cosmic rays and meteorites) in the hexagon. Identification of primary lithic components contributing to each breccia lithology follows from Fig. 3. The LG and white clast lithologies are identified as part of the "megaregolith" because they exist as relatively large clasts (>~cm-sized) having little evidence of prolonged residence in the uppermost lunar surface layers. A higher proportion of components in the DG and impact melt lithologies derive from shallow depths in the lunar regolith.

various components within it. The paucity of indicators of regoltih exposure in the LG lithology suggests its components were mostly igneous rocks prior to impact comminution and thermal metamorphism, but the range of mineral compositions observed in LG suggest it is from an older-generation breccia. The well-defined Ar–Ar age and low trapped gas content of the clast is consistent with its existence as a single clast prior to an energetic impact event that totally outgassed its Ar. Lithification of LG occurred prior to assembly of the Y-86032 breccia, and is dated at $4.10 \pm 0.02$ Ga by the Ar–Ar age plateau obtained for sample ,28.

Textural relationships show that the DG-lithology was formed by impact lithification of regolith composed of several highland igneous/metamorphic components, impact melt clasts, and minor contributions of mare basalts. The presence of impact melt clasts in DG suggests that some of these components had experienced impact events before final lithification. Nevertheless, this lithology also was dominantly anorthositic. Preservation of mineral and lithic clasts of significant size suggests lithification of a relatively immature regolith. Lithification of DG is judged to have occurred in a less energetic impact than for LG because Ar outgassing was incomplete on lithification. As presented in detail above, the Ar–Ar age pattern during stepwise heating suggests the most probable time of lithification was $3.8 \pm 0.1$ Ga ago.

The final impact event recorded texturally produced the IM-lithology that cuts across both DG and LG. IM is essentially a melted version of DG. Because IM also was not completely degassed during lithification, we suggest that impact melting was by a local event followed by relatively rapid cooling of the impact melt. The most probable interpretation of the data for sample ,33 IM gives a degassing/melting age of ~3.8 Ga. Thus, the Ar–Ar age spectra of the IM and DG lithologies, as recorded in subsamples ,33 and ,30, respectively, are consistent with formation of the melt during breccia assembly ~3.8 Ga ago.

The Rb–Sr tie-line age of $4.00 \pm 0.17$ Ga for ,33 IM with ,28 LG probably reflects only partial resetting during the ~3.8 Ga breccia-assembly event. Thus, final breccia assembly probably occurred near the end of the hypothesized ~3.8–3.9 Ga lunar cataclysm (Tera et al., 1974; Ryder, 2002). The existence of older impact events at ~4.1 Ga and probably at ~4.25–4.36 Ga makes ambiguous the extension of the cataclysm hypothesis to the lunar farside.

Cratering studies show that monomict breccias are found on the floors and along the walls of impact craters (Kieffer and Simonds, 1980; Stöffler, 1981). From this observation, Nyquist et al. (1986) suggested that polymict eucrites likely formed by impact excavation to the surface of their parent body, whereas monomict ordinary eucrites more likely formed near crater floors or along crater walls. By analogy, a geologic setting for the LG clast below a crater floor or along a crater wall prior to its excavation and mixing with DG regolith is a plausible explanation for its lithification in a relatively energetic event. A post-impact location below a crater floor or in a crater wall would account for prolonged and thorough outgassing following its formation as well as its shielding from regolith inputs.

Although it is impossible to unambiguously specify the geologic setting for formation of Y-86032/Y-82192/3 itself, we know that it was deeply buried following breccia assembly ~3.8 Ga ago. The textural relationships suggest a fast-moving stream of melt penetrated into more slowly moving, possibly stationary, material. Again, a crater floor or wall is a plausible location for this scenario, since again the impact breccia remained shielded from regolith inputs. In spite of uncertainty concerning the exact geologic setting of its lithification, it is significant that Y-86032/Y-82192/3 records only a few major impacts during its residence in the megaregolith, and that the evidence of earlier impacts was retained during subsequent impacts. Finally, the breccia was exhumed and launched into space ~7–10 Ma ago.

### 6.4. Initial $\varepsilon_{Nd}$ of the protolithic lunar crust

If the LREE enrichment that is characteristic of lunar anorthosites was produced early in lunar history from an LMO of initially chondritic relative REE abundances, one would expect a zero, or more likely, negative $\varepsilon_{Nd}$ value. This is because, by definition, $\varepsilon_{Nd}$ is the deviation of initial $^{143}Nd/^{144}Nd$ measured for a sample from the value that would exist in a reservoir of the same age that always had been characterized by chondritic relative REE abundances. By convention, one usually calculates $\varepsilon_{Nd\ CHUR}$ relative to an interlaboratory-adjusted initial $^{143}Nd/^{144}Nd$ value for a Chondritic Uniform Reservoir, the parameters of which have been given by Jacobsen and Wasserburg (1984). For the isochron for the combined ,28 and ,44 data (Fig. 8), $\varepsilon_{Nd\ CHUR}$ is $+0.19 \pm 0.13$. However, $\varepsilon_{Nd}$ for these data is more appropriately calculated as $\varepsilon_{Nd\ \ HED} = -0.64 \pm 0.13$ relative to initial $^{143}Nd/^{144}Nd$ obtained at the Johnson Space Center (JSC) for HED meteorites (Nyquist et al., 2004). The difference between the two values is shown in Fig. 17, where all $\varepsilon_{Nd}$ values are shown relative to $\varepsilon_{Nd\ HED} = 0$.

Fig. 17 compares $\varepsilon_{Nd}$ values for Y-86032 subsamples to literature data for Apollo 16 FANs, Apollo 15 and 17 norites, and KREEP-rich samples. The reference datum is "HED PB" at $\varepsilon_{Nd} = 0$ at 4.567 Ga ago. To maintain self-consistency within the data set, all the Nd-isotopic data shown in the figure are from the JSC lab. Thus, for example, recently measured JSC Nd isotopic data for 60025 are shown plotted at an age of $4.42 \pm 0.02$ Ga as determined by Carlson and Lugmair (1988). Similarly, recent JSC data for 67075 are shown plotted at the Ar–Ar age of $3.98 \pm 0.05$ Ga (Turner et al., 1973; Shih et al., 2005). The new data for the (,28 + ,44) combined isochron (Fig. 8), like that for the KREEP and norite samples, are consistent with radiogenic growth with $^{147}Sm/^{144}Nd$ $(\mu) = 0.17$ from HED PB at 4.56 Ga ago. The data for ,116 GC, plotted at the $^{39}Ar$–$^{40}Ar$ age of ,116 GC, lie below this evolution line and require evolution in a reservoir of lower Sm/Nd ratio, i.e., a more LREE-enriched reservoir. An evolution line for $\mu = 0.13$ calculated for the Sm and Nd abundances in anorthosite Dhofar 489 d2 (Takeda et al., 2006; REE pattern shown in Fig. 7) intersects chondritic evolution within error limits of 4.567 Ga ago. This $\mu$-value may be considered a limiting case approached only by $\mu$ ~0.14 in plagioclase separates from FANs 60025 and 62236 (Carlson and Lugmair, 1988; Borg et al., 1999). Nevertheless, the probable origin of both Y-86032 and Dhofar 489 on the lunar farside suggests that comparison of the Nd-isotopic evolution in the Y-86032 lithologies to that in a farside anorthosite is the logical choice.

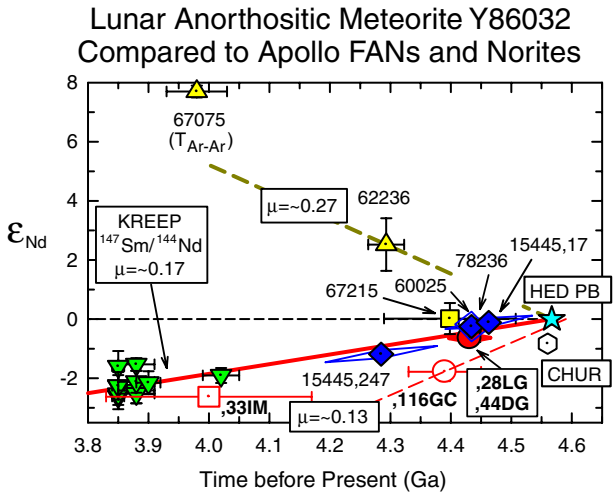


Fig. 17. Initial $\varepsilon_{Nd}$ values for Y-86032 (,28 LG + ,44 DG) and ,116 GC compared to literature data for Apollo 16 FANs (Carlson and Lugmair, 1988; Borg et al., 1999; Norman et al., 2003), Apollo 15 and 17 norites (Nyquist et al., 1981; Shih et al., 1993), and KREEP (Nyquist et al., 2001) normalized to values that would exist in a "chondritic" reservoir as determined from measurements of many eucrites in the JSC lab (Nyquist et al., 2004) and shown by "HED PB" at 4.567 Ga ago. $^{143}Nd/^{144}Nd$ for HED PB is higher than our interlaboratory-adjusted value for CHUR (Jacobsen and Wasserburg, 1984) by 0.8 $\varepsilon$-units. The lunar data shown are from the JSC lab except for the age of 60025 (Carlson and Lugmair, 1988). The new data for the (,28 + ,44) combined isochron like that for the norite and KREEP samples are consistent with radiogenic growth with $^{147}Sm/^{144}Nd$ $(\mu) = 0.17$ from HED PB at 4.56 Ga ago. The data for ,116 GC, plotted at the $^{39}Ar$–$^{40}Ar$ age of ,116 GC lie below this evolution line and require evolution in a reservoir of lower Sm/Nd ratio, i.e., a more LREE-enriched reservoir. An evolution line for $\mu = 0.13$ calculated for the Sm and Nd abundances in anorthosite Dhofar 489 d2 (Takeda et al., 2006) intersects chondritic evolution within error limits of 4.567 Ga ago. The datum for ,33 IM is shown plotted at the Rb–Sr tie-line age of $4.00 \pm 0.17$ Ga (Fig. 9).

Importantly, the Y-86032 Nd-isotopic data do not imply derivation of their anorthositic lithologies from an earlier LREE-depleted reservoir, as do many of the data for Apollo 16 FANs. Significantly, this statement holds both for the dominant An93 anorthositic component in ,28 LG as well as for the dominant An97 anorthositic component in ,116 GC. Interestingly, An93 anorthosite shares some characteristics with Mg-suite norites (e.g., An number, initial $\varepsilon_{Nd}$ ). An97 anorthosite shares several characteristics with Apollo 16 FANs (e.g., An number, initial $^{87}Sr/^{86}Sr$ to be discussed later), but An97 anorthosite is distinguished from ordinary FANs in having an $\varepsilon_{Nd}$ value that makes it a candidate for a crystallization product from the Lunar Magma Ocean (LMO) whereas ordinary FANs do not. The reason why

Apollo 16 FANs appear to have higher $\varepsilon_{Nd}$ values $\geqslant 0$ is not well understood. The possibility of partial Nd-isotopic equilibration related to significant exogenic thermal inputs into the lunar crust from major basin-forming impacts on the lunar nearside is intuitively attractive, but difficult to justify in detail. The possible "late" generation of some anorthositic highland lithologies not directly connected to the LMO, i.e., serial magmatism (Walker, 1983), therefore needs to be retained as a working hypothesis.

Fig. 17 also shows $\varepsilon_{Nd}$ for ,33 IM calculated at the Rb–Sr tie-line age of 4.00 ± 0.17 Ga (Fig. 9). The calculated datum plots close to the evolution line corresponding to $^{147}Sm/^{144}Nd$ ~0.17 in KREEP source regions. The low Th abundance in Y-86032 excludes the presence of significant KREEP in the impact melt, but 'Mg-suite' norites and troctolites also have source regions with $^{147}Sm/^{144}Nd$ ~0.17 (Shih et al., 1993). Thus, mixing end-members for the IM impact melt, in addition to components present in the LG breccia, may include rocks that, like KREEP and the Mg-suite, contain an urKREEP component.

### 6.5. Initial $^{87}Sr/^{86}Sr$ of the protolithic lunar crust

The new Sr isotopic data of Y-86032, combined with data for lunar anorthosites and "benchmark" values of initial $^{87}Sr/^{86}Sr$ for more primitive objects allow reassessment of Sr-isotopic constraints on lunar crustal evolution. Fig. 9 compares $^{87}Sr/^{86}Sr$ for the Y-86032 lithologies and lunar FANs. As noted in Section 5.2, $^{87}Rb/^{86}Sr$ and $^{87}Sr/^{86}Sr$ values for all of the Y-86032 lithologies, even the DG and IM lithologies, are low relative to lunar surface values represented in the Apollo samples. Lunar soils from Apollo 15, 16, and 17 contain highland rock components and provide a standard of comparison. Among several soils from each site analysed by Nyquist et al. (1973, 1974), for example, the lowest values were for soils 15101, 63501, and 75061. Measured $^{87}Rb/^{86}Sr$ values in these soils were 0.0908, 0.0287, and 0.0193, respectively, i.e., off scale for Fig. 9. Additionally, the highland soil 22001 from the Luna 20 site had a $^{87}Rb/^{86}Sr$ ratio of 0.0329. Among these sites from which we have returned samples, the Apollo 16 and Luna 20 soils are most typical of the lunar highlands. In contrast to soils from these sites, the highest $^{87}Rb/^{86}Sr$ values found for the Y-86032 lithologies were 0.00576 for the ,44 DG regolith sample and 0.00639 for the ,30 impact melt sample, ~5× lower than for the Apollo 16 and Luna 20 highland soils. Since Rb is one of the KREEP elements, the low Rb content of the DG "regolith" sample is further evidence that the parental terrain of Y-86032 was far from the KREEP-rich PKT terrain on the lunar nearside.

Mg-suite rocks are a prominent crustal component at least at the Apollo 15 and 17 sites, and Mg-suite norites have Rb/Sr ratios that are similar to those of highland soils. Reasons for this observation may vary from site to site, and arguably reflects the influence of the PKT either during petrogenesis of some crustal lithologies, or as a source for physical admixture of PKT-derived material. No Apollo highland soil so far analysed has a $^{87}Rb/^{86}Sr$ ratio as low as those of the DG and IM "regolith" lithologies of Y-86032. This may be a consequence of the lack of an Mg-suite crustal lithology at the Y-86032 site, physical distance from the PKT, or both. Interestingly, the An93 anorthosite component present in LG has some similarities to Mg-suite norites, and appears to fulfill some of the geochemical and isotopic roles taken by nearside Mg-suite rocks. The An contents of the plagioclases are similar, and, as shown above, the Sm–Nd systematics of An93 anorthosites also are similar to those of some Mg-suite norites. The Rb–Sr isotopic systematics are dramatically different, however, as shown in Table 6. Whereas Fig. 9 compares the Rb–Sr systematics of the farside(?) anorthosites to FANs, Table 6 extends the comparison to the known crustal norites. With regard to Table 6, we note that because the Rb–Sr isotopic systematics of pyroxenes separated from lunar norites often prove to be disturbed by "young" events, the initial $^{87}Sr/^{86}Sr$ values given in the table have been calculated for plagioclase and whole rock analyses judged to be free of such disturbances. The average $^{87}Rb/^{86}Sr$ and $^{87}Sr/^{86}Sr$ values given for each norite have been separately calculated from whole rock analyses only, and represent a different and more restricted data set than do the calculated initial $^{87}Sr/^{86}Sr$ values. Thus initial $^{87}Sr/^{86}Sr$ values calculated from the whole rock $^{87}Rb/^{86}Sr$ and $^{87}Sr/^{86}Sr$ values in the table will be slightly different from the more accurate values in the table. Nevertheless, the implications of the data are the same.

Traditionally, Apollo FANs have been used to estimate the lunar initial $^{87}Sr/^{86}Sr$ ratio, and form the standard of comparison as in Fig. 9. A least squares fit to the FAN data define a lunar initial $^{87}Sr/^{86}Sr$ (I(Sr)) = 0.699066 ± 43 for a "best fit" age of 4.62 ± 0.89 Ga. Table 6 shows that essentially the same initial $^{87}Sr/^{86}Sr$ value is derivable from either of the two farside(?) anorthosites considered separately, or from Apollo norites, if a primary age of differentiation of 4.567 Ga is assumed for the latter. Most of the norite data in Table 6 are from earlier generation analyses, and the analytical uncertainties on the measured $^{87}Sr/^{86}Sr$ ratios were considerably higher than for current data. Note especially that for the An97 and An93 anorthosites the calculated values of I(Sr) are insensitive to the assumed lunar age within the interval of 4.1 Ga, the Ar–Ar age of the LG lithology, to 4.567 Ga. The average calculated initial $^{87}Sr/^{86}Sr$ values for WR and plagioclase analyses are within error limits of the initial lunar value for any age within these broad limits. Not so for the norites, which because of their much higher $^{87}Rb/^{86}Sr$ ratios only give the lunar initial $^{87}Sr/^{86}Sr$ ratio at an age of primary differentiation of 4.567 Ga. The good agreement of I(Sr) for FANS with $I(Sr)_{4.567}$ values for An97 anorthosite (0.699058 ± 23), An93 anorthosite (0.699051 ± 5) and the cited norites (0.699060 ± 47) cannot be a coincidence, in our opinion. Thus, although norites are widely assumed to have formed as plutons within an anorthositic crust (e.g., James, 1980), they nevertheless carry the Sr-isotopic signature of the primary lunar differentiation.

Table 6
Rb–Sr isotopic systematics of farside(?) anorthosites compared to norites

| Sample | $^{87}Rb/^{86}Sr$[c] | $^{87}Sr/^{86}Sr$[c] | $I(Sr)_{4.1}$[d] | $I(Sr)_{4.43}$[d] | $I(Sr)_{4.567}$[d] |
|---|---|---|---|---|---|
| An97 anorthosite | | | | | |
| Y-86032,116 GC | 0.00211 | 0.699213 | 0.699088 | 0.699078 | 0.699073 |
| Y-86032,133 W - Pl | 0.00161 | 0.699148 | 0.699053 | 0.699045 | 0.699042 |
| Avg | | | 0.699070 | 0.699061 | 0.699058 |
| St Dev | | | 0.000025 | 0.000023 | 0.000023 |
| An93 anorthosite | | | | | |
| Y-86032,28 LG | | | | | |
| WR | 0.00121 | 0.699135 | 0.699063 | 0.699057 | 0.699055 |
| Plag | 0.00109 | 0.699120 | 0.699056 | 0.699050 | 0.699048 |
| Avg | | | 0.699059 | 0.699054 | 0.699051 |
| St Dev | | | 0.000006 | 0.000005 | 0.000005 |
| Norites | | | | | |
| 15445,17[a] | 0.03240 | 0.701190 | 0.699317 | 0.699140 | 0.699067 |
| 15445,247[a] | 0.03580 | 0.701380 | 0.699325 | 0.699164 | 0.699097 |
| 15455,228[a] | 0.02380 | 0.700620 | 0.699274 | 0.699075 | 0.698992 |
| 78236[b] | 0.02398 | 0.700570 | 0.699200 | 0.699119 | 0.699085 |
| Avg | | | 0.699279 | 0.699124 | 0.699060 |
| St Dev | | | 0.000057 | 0.000038 | 0.000047 |

[a] Shih et al. (1993).
[b] Nyquist et al. (1981).
[c] Values given are averages for whole rock analyses reported in the cited references.
[d] Initial $^{87}Sr/^{86}Sr$ from plag and whole rock analyses for the subscripted ages (Ga).

## 7. Conclusions and implications

This combined mineralogical, chemical, and chronological study of Y-86032 suggests formation of the lithologies present in it within the farside lunar crust (“protolith”) at or before $4.43 \pm 0.03$ Ga ago. This age is based on the Sm–Nd age of the combined LG and DG lithologies and the Ar–Ar age of ,116 GC. It also derives some support from the Ar–Ar age spectra of two impact melt samples from the breccia, both of which give maximum Ar–Ar ages of ~4.35–4.37 Ga for individual temperature steps. The close agreement of these maximum ages with the age of ,116 GC, and also with the Sm–Nd age of combined LG and DG lithologies seems more than coincidental.

We interpret the observation that the Sm–Nd-isotopic data for LG and DG lithologies lie on a single Sm–Nd isochron within error limits to mean that the farside(?) protolith from whence Y-86032 came contained only a limited range of mostly cogenetic lithologies. Additionally, the initial $^{143}Nd/^{144}Nd$ present in the protolith when it solidified is consistent with crustal formation via plagioclase flotation on the LMO. Furthermore, the coincidence in initial $^{87}Sr/^{86}Sr$ for ancient crustal samples from the lunar nearside (Apollo 16 FANs) and probably the lunar farside (Y-86032 lithologies) is consistent with the concept of an LMO that initially was global in extent.

Some of the impact lithologies in Y-86032 clearly were formed prior to the hypothesized cataclysmic bombardment of the lunar surface about 3.9 Ga ago (Tera et al., 1974; Ryder, 2002), as shown most clearly by the $4.10 \pm 0.02$ Ga Ar–Ar age of LG lithology ,28. The >4.35 Ga Ar–Ar age of ,116 GC also may be related to impact processes, but more probably this age and the oldest age observed in sample ,133 represent partial retention of an original crystallization age similar to the ~4.43 Ga Sm–Nd age of the LG and DG lithology.

The presence of clasts in Y-86032 with differing Ar–Ar ages implies multiple impact heating events. Formation of the Y-86032 breccia and impact melt likely occurred ~3.8 Ga ago within the period of the proposed lunar cataclysm. The question arises as to how older Ar-retention ages survived the hypothesized later cataclysmic bombardment (*cf.* Hartmann, 2003). That Y-86032 spent most of its existence deeply buried in a megaregolith far distant from basin-forming impacts likely contributed to its survival.

The results of this investigation strongly support earlier suggestions of a lunar farside origin for Y-86032. The variety of clast types in Y-86032, particularly in the DG regolith lithology, reflects igneous, impact, and metamorphic processes occurring on the lunar highland crust. Nevertheless, in spite of this evidence of multiple impacts and mixing, the extremely low Th and Fe contents in the Y-86032 breccia indicate that mixing was mostly limited to components from the Feldspathic Highland Terrain (FHT), and exclusive of material from the Procellarum KREEP Terrain (PKT). Furthermore, the LG lithology of very low Th content contains a restricted suite of rocks, some of which have not been found in previous studies. The dominant primary rock type present in LG is an anorthosite containing ~An93 plagioclase. Because the plagioclase occurs only as individual mineral grains, we are unable to specify a corresponding mg′ number. However, the combination of norite-like An93 plagioclase, KREEP-like $\varepsilon_{Nd}$, FAN-like initial $^{87}Sr/^{86}Sr$, and very low $^{87}Rb/^{86}Sr$ found

for "An93 anorthosite" is unique among lunar samples. A second unique component of LG, not yet isotopically characterized, has much lower An ~83 and low mg′ ~40–50 as measured for an individual lithic clast in LG. These characteristics of one of its clasts place the place of origin of Y-86032 within the FHT with a higher probability of a farside origin than an origin within the nearside central lunar highlands visited by Apollo 16. The strongly negative (for its age) $\varepsilon_{Nd}$ value of the FAN-like ,116 gray clast is unlike that so far found for Apollo 16 FANs of the nearside central highlands, although the Sr-isotopic data appear to be identical. This suggests that the Nd-isotopic systematics of Apollo 16 FANs have been disturbed by external effects, possibly connected with heavy impact bombardment of the lunar nearside.

Assuming a farside origin for Y-86032, the isotopic data presented here provide a strong hint of an early hemispheric divergence in lunar geochemical evolution. We suggest that during or immediately after initial magma ocean crystallization on the nearside hemisphere a residual magma may have become physically separated from already crystallized phases (mafic cumulates?) that were more Fe-rich than the bulk magma. The mafic phases would be LREE-depleted, whereas the residual magma would be enriched in what has come to be known as the urKREEP component. Such a separation may have been a consequence of gravitational settling of mafic phases combined with stochastic accretionary processes. Following such an event, there may have been a period of super-chondritic radiogenic growth of $^{143}Nd$ in that volume of the moon enriched in mafic phases and thus LREE-depleted. Another major, accretionary, impact into that volume of the moon may have created a new magma sea, perhaps in the region now occupied by the nearside central highlands. Anorthosites which floated to the top of the nearside magma sea, perhaps as late as ~4.42 Ga ago, would crystallize with a net enrichment of $^{143}Nd$ relative to that in undifferentiated chondritic material, i.e., would have positive $\varepsilon_{Nd}$ as observed for nearside FANs. They would be relatively Fe-rich and have lower REE than anorthosites crystallizing from a magma ocean of bulk lunar composition because they would come from a derivative portion of the ocean from which some of the REE had been physically removed. The crystallization products of the complementary trace-element-enriched portion of this scenario would show little isotopic evidence of separation from the mafic component because parent/daughter element ratios would be little affected. Hypothetically, Mg-suite rocks might belong to the latter category, thereby explaining their "memory" of the initial $^{87}Sr/^{86}Sr$ ratio at 4.567 Ga ago in spite of having relatively high $^{87}Rb/^{86}Sr$ ratios. Attempts to explain *all* trace element enrichments of lunar rocks, even the modest ones observed in Mg-suite rocks, via contamination with urKREEP may prove misguided.

These ideas are speculative, but are subject to testing with other geochemical parameters and samples. They appear to be consistent with two "evolving views" expressed by Korotev (2005) in his review of the geochemical data from lunar meteorites in the context of the global geochemical data provided by spacecraft: (a) "No global, subcrustal layer of magma-ocean residuum (KREEP)" (Korotev, Section 5.1); (b) "No magesian-suite "highland" rocks" (Korotev, Section 5.2). Korotev (p. comm.) notes that his discussion pertains to magnesian suite rocks as found in the Apollo collections, more commonly called Mg-suite rocks. Tompkins and Pieters (1999) presented evidence from Clementine data for candidate mafic plutons in the highlands, but noted that mafic lithologies identified among highland crater central peaks are typically more anorthositic than the average for large Mg-suite samples of the Apollo collections. Samples containing pristine primary rock types returned from the farside lunar highlands would be very useful to test these ideas and to determine the crystallization path(s) of the LMO.

Even accepting the possibility of a nearside/farside dichotomy in development of the LMO, the occurrence of positive $\varepsilon_{Nd}$ values and compositional variability among samples of nearside ferroan anorthosite remains poorly understood. Haskin et al. (1981) in their study of compositional variability among lunar anorthosites concluded: "...we find it difficult to account for the compositions (and mineralogy) of lunar anorthosites in terms of the simple fractional crystallization model which is generally proposed to have produced anorthosites from the lunar magma ocean". They suggested that mafic phases in anorthosites accumulated from a magma ocean might be expected to be modally more abundant than observed in the most plagioclase-rich anothosites, and that these mafic phases had been removed via reheating events. Appealing to impact tectonics as a heat source, they suggested that such processes might be "...regarded as an active, integral, initial part of the overall mechanism that produced lunar anorthosites..." They were led to that suggestion by noting that the low $^{87}Sr/^{86}Sr$ in FANS required very early separation of Rb from Sr in anorthosites. In their mechanism, which is local in nature, one might therefore expect to find some FANs from which such early removal of Rb had not occurred. The reader may wish to consider: (a) The location of "norite" 15445 squarely within the FAN region of Fig. 3, and (b) its relatively high "norite-like" Rb/Sr ratio, but primordial $^{87}Sr/^{86}Sr$ at 4.567 Ga ago (Table 6). Perhaps these observations are a manifestation of the processes suggested by Haskin et al. (1981), and perhaps the positive $\varepsilon_{Nd}$ values exhibited by some FANs are a further manifestation of such local processes. These ideas require quantitative evaluation before acceptance, but clearly more work is required to fully understand the implications of lunar anorthosites for ideas of lunar formation and evolution. The present work suggests that expanding the sampled anorthosite suite to include samples of pristine farside anorthosites would materially aid in that endeavor.

**Acknowledgments**

This research was supported by a Grant-in-Aid for Scientific Research from the Ministry of Education, Science and Technology, Japan, No. 12740300 (A.Y.) and by NIPR Research Project Funds, P-8 (Evolution of the early Solar System materials). Research at the Johnson Space Center was supported by NASA RTOP 344-31 to L. Nyquist, D. Bogard, and G. McKay. We thank H. Kojima for discussion and the sample preparation of Y-86032. Thoughtful and detailed reviews by R. Korotev, Y. Ikeda, and an anonymous reviewer as well as editorial handling by G. Herzog are appreciated. Finally, this paper is dedicated to the memory of Larry Haskin, for his many examples of leadership in lunar and planetary science, but most of all for the intellectual honesty that he so consistently insisted upon.

*Associate editor:* Gregory F. Herzog

## Appendix A. $^{37}$Ar Half-life and $^{39}$Ar/$^{37}$Ar correction factors

The complex, brecciated nature of Y-86032 combined with its anorthositic composition place stringent demands on radiometric dating techniques. For example, the $^{39}$Ar–$^{40}$Ar dating technique is based on the reaction $^{39}$K (n, p) $^{39}$Ar. However, $^{39}$Ar is also produced from the reaction $^{42}$Ca (n, α) $^{39}$Ar. Thus, a correction for Ca-produced $^{39}$Ar must be applied. This is done by multiplying $^{37}$Ar produced in the reactor from the reaction $^{40}$Ca (n, p) $^{37}$Ar by a $^{39}$Ar/$^{37}$Ar factor experimentally determined for the reactor used. Corrections to $^{39}$Ar of 25–50% are typical for samples with K/Ca ratios <0.001, like lunar anorthosites. Yet, many earlier reports of Ar–Ar ages of lunar anorthosites did not discuss uncertainties in the $^{39}$Ar corrections that were applied. It is well known that the $^{39}$Ar/$^{37}$Ar correction factor varies among neutron reactors, but the extent of the variation among different irradiations in the same reactor apparently has not been investigated in detail. Further, because $^{37}$Ar decays rapidly, the measured $^{37}$Ar must be corrected back to the time of irradiation, and any uncertainty in the $^{37}$Ar half-life affects the correction to $^{39}$Ar, and thus the age. Measurements of the $^{37}$Ar half-life reported in the literature were all determined by counting the rate of $^{37}$Ar decay, and vary by a few percent. Although most labs that determine Ar–Ar ages use a half-life of 35.1 days as reported by Stoenner et al. (1965), past publications of the Chart of the Nuclides have given various half-lives representing averages of different determinations.

In order to accurately determine the $^{39}$Ar/$^{37}$Ar correction factor for our low-K samples, to confirm the $^{37}$Ar half-life by a non-counting technique, and to examine possible variations in the $^{39}$Ar/$^{37}$Ar correction factor among different irradiations in the same reactor, we included two samples of a pure $CaF_2$ crystal in each of five neutron irradiations made over a period of five years. Each irradiation was conducted in the same insertion port location of the University of Missouri Research Reactor (MURR). For each sample in a pair of $CaF_2$ samples, we measured the Ar isotopic composition at different times after irradiation. The difference in measured $^{39}$Ar/$^{37}$Ar ratios in these sample pairs depends solely on the decay of $^{37}$Ar. (A correction is applied for the decay of $^{39}$Ar, but this is very minor). Thus, precise measurements of the $^{39}$Ar/$^{37}$Ar ratio by mass spectrometry gives a determination of the $^{37}$Ar half-life by a technique completely different from the counting techniques previously used, as well as the $^{39}$Ar/$^{37}$Ar correction factor that must be applied to the meteorite data.

### *A.1. Half-life of $^{37}$Ar*

The measured $^{39}$Ar/$^{37}$Ar ratios, calculated $^{37}$Ar half-life, and determined $^{39}$Ar/$^{37}$Ar correction factors for the five pairs of $CaF_2$ samples are given in Table A1. Uncertainties listed for the $^{39}$Ar/$^{37}$Ar factors include errors in measured isotopic ratios and blank corrections. Time differences between analyses ($\Delta$–$T$) of each $CaF_2$ sample in a pair varied between 57 and 102 days, approximately 2 to 3 half-lives of $^{37}$Ar. This time was used to decay-correct the $^{39}$Ar/$^{37}$Ar ratio for the second sample in each pair to match the $^{39}$Ar/$^{37}$Ar ratio of the first sample in each pair. In this correction, the value of the $^{37}$Ar half-life was considered a variable, and the half-life values listed in Table A1 are those required to match $^{39}$Ar/$^{37}$Ar ratios for each pair of $CaF_2$ samples. The five half-life determinations show a tight grouping and give an average value of $35.06 \pm 0.04$ ($1\sigma$) days. This value is the same within respective uncertainties of the $^{37}$Ar half-life of $35.1 \pm 0.1$ days reported by Stoenner et al. (1965).

### *A.2. Variability in $^{39}$Ar/$^{37}$Ar factors*

The average $^{39}$Ar/$^{37}$Ar correction factor for these five irradiations is $7.43 \pm 0.21 \times 10^{-4}$, which becomes

Table A1
Data determined from pairs (#1 & #2) of irradiated $CaF_2$ samples

| Irrad. No. | $\Delta T$ (days) | Measured $^{39}$Ar/$^{37}$Ar & ± (×10$^4$) | | $^{37}$Ar t1/2 (days) | $^{39}$Ar/$^{37}$Ar factor ×10$^4$ |
|---|---|---|---|---|---|
| | | #1 | #2 | | |
| 97A | 100 | 519.29 ± 0.26 | 77.742 ± 0.033 | 35.06 | 7.495 ± 0.078 |
| 98A | 76 | 873.39 ± 0.56 | 193.75 ± 0.13 | 35.10 | 7.364 ± 0.074 |
| 99C | 57 | 346.41 ± 0.55 | 108.50 ± 0.11 | 35.01 | 7.681 ± 0.077 |
| 00A | 102 | 915.80 ± 1.18 | 121.19 ± 0.15 | 35.02 | 7.104 ± 0.137 |
| 02A | 93 | 519.29 ± 0.26 | 77.742 ± 0.033 | 35.10 | 7.495 ± 0.075 |

$7.51 \pm 0.13 \times 10^{-4}$ if we omit the value for sample 00A, which is considerably lower than the others and possesses the largest uncertainty. Although $^{37}Ar$ half-lives derived from the five pairs of $CaF_2$ samples show a spread of only 0.26%, the determined $^{39}Ar/^{37}Ar$ correction factors show a total spread of 7.7%, which is considerably larger than the individual uncertainty of ~1% for four of the five factors. The larger variation is thus produced by different irradiations, not by a variation among individual samples, and is not explained by variable K contamination on the surface of the $CaF_2$, as suggested by McDougall and Harrison (1999).

Each $^{39}Ar/^{37}Ar$ factor in Table A1 was calculated by forcing the $^{39}Ar/^{37}Ar$ ratio for the two samples in each $CaF_2$ pair to be equal, and thus assumes the $^{37}Ar$ half-life has the value determined for that irradiation. If, instead, we use the average determined $^{37}Ar$ half-life of 35.06 d, the difference in $^{39}Ar/^{37}Ar$ correction factors for the two $CaF_2$ samples in each pair still remains small compared to the difference among $^{37}Ar/^{39}Ar$ factors reported in Table A1 for each pair. To force the $^{39}Ar/^{37}Ar$ factors for the five irradiations to be equal would require significant variations in the actual $^{37}Ar$ half-life, which cannot be true. Thus, we conclude that these irradiations actually give slightly different values of the $^{37}Ar/^{39}Ar$ correction factor, in spite of the fact that the irradiations were conducted in a similar manner. We believe that we can discount several specific factors as causes for the observed $^{39}Ar/^{37}Ar$ variation. First, the $^{37}Ar$ decay correction applied for each irradiation includes decay of $^{37}Ar$ during the irradiation, in addition to $^{37}Ar$ decay after the irradiation. Secondly, samples in each $CaF_2$ pair were irradiated in adjacent positions within the same quartz tube, except sample 98A, where the two samples were irradiated in the same relative positions of adjacent quartz tubes. Further, irradiations 97A–99C were made with boron–nitride shielding around the samples to absorb thermal neutrons, whereas the irradiations 00A and 02A had no thermal shielding. (We would not expect changes in thermal neutron flux to affect the neutron rigidity in the MeV energy range.)

We believe that the variable $^{39}Ar/^{37}Ar$ correction factors can be explained by characteristics of reactor operation. The excitation functions (i.e., cross section as a function of energy) for production of $^{39}Ar$ and $^{37}Ar$ by neutron capture on Ca are not identical. Thus, the specific $^{39}Ar/^{37}Ar$ correction factor also depends upon neutron rigidity, i.e., the flux of fast neutrons as a function of energy. Among various reactors that have been used for $^{39}Ar/^{40}Ar$ dating, correction factors of $\sim(6.4–12) \times 10^{-4}$ have been reported (McDougall and Harrison, 1999). The MURR reactor contains eight fuel elements in a cylindrical array, and periodically one fuel element at a time is replaced. (Fission products build up in old fuel elements and slow down the chain reaction by adsorbing neutrons.) Control rods are used to maintain a constant thermal neutron flux during each 6.5-day neutron-generating cycle. Our irradiation position is located on the outside edge of the reactor core. Thus, depending on whether the nearest fuel element to our irradiation position is new or old, and on the relative position of the control rods in the core, the neutron rigidity can vary at our irradiation location. We believe this is the explanation for the observed ~8% variation in $^{39}Ar/^{37}Ar$ correction factors in Table 1. We point out that such variations are likely to occur in all reactors, and thus any analysis of samples with very low K/Ca ratios should document such variations, and not simply assume that one value determined for a given reactor is invariant.

Because we did not include $CaF_2$ samples in every University of Missouri irradiation that contained low-K samples, we adopt a standard $^{39}Ar/^{37}Ar$ correction factor of $7.5 \pm 0.2 \times 10^{-4}$ for the sample analyses reported here. We believe these procedures have improved both the precision and accuracy of the Ar–Ar ages of the various Y-86032 lithologies.

## References


Alibert, C., Norman, M.D., McCulloch, M.T., 1994. An ancient Sm–Nd age for a ferroan noritic anorthosite clast from lunar breccia 67016. *Geochim. Cosmochim. Acta* **58**, 2921–2926.

Armstrong, T.W., Alsmiller, R.G., 1971. Calculation of cosmogenic radionuclides in the Moon and comparison with Apollo measurements. *Proc. Lunar Sci.* **2**, 1729–1745.

Arvidson, R., Drozd, R., Guiness, E., Hohenberg, C., Morgan, C., Morrison, R., Oberbeck, V., 1976. Cosmic ray exposure ages of Apollo 17 samples and the age of Tycho. *Proc. Lunar Sci.* **7**, 2817–2832.

Bischoff, A., Palme, H., Weber, H.W., Stöffler, D., Braun, O., Begemann, F., Wänke, H., Ostertag, R., 1987. Petrography, shock history, chemical composition and noble gas content of the lunar meteorites Yamato-82192 and -82193. *Mem. Natl. Inst. Polar Res., Spec.* **46**, 21–42.

Bischoff, A., Stöffler, D., 1992. Shock metamorphism as a fundamental process in the evolution of planetary bodies: information from meteorites. *Eur. J. Mineral.* **4**, 707–755.

Bogard, D.D., Nyquist, L.E., Bansal, B.M., Garrison, D.H., Wiesmann, H., Herzog, G.F., Albrecht, A.A., Vogt, S., Klein, J., 1995. Neutron-capture $^{36}Cl$, $^{41}Ca$, $^{36}Ar$, and $^{150}Sm$ in large chondrites: evidence for high fluences of thermalized neutrons. *J. Geophys. Res.* **100**, 9401–9416.

Bogard, D.D., Garrison, D.H., Nyquist, L.E., 2000a. Ar-39–Ar-40 ages of lunar highland rocks and meteorites (abstract). *Lunar Planet. Sci.* **31**, 1138, CD-ROM.

Bogard, D.D., Garrison, D.H., McCoy, T.J., 2000b. Chronology and petrology of silicates from IIE iron meteorites: evidence of a complex parent body evolution. *Geochim. Cosmochim. Acta* **64**, 2133–2154.

Borg, L.E., Norman, M., Nyquist, L., Bogard, D., Snyder, G., Taylor, L., Lindstrom, M., 1999. Isotopic studies of ferroan anorthosite 62236: a young lunar crustal rock from a light-rare-earth-element-depleted source. *Geochim. Cosmochim. Acta* **63**, 2679–2691.

Carlson, R.W., Lugmair, G.W., 1981. Time and duration of lunar highlands crust formation. *Earth Planet. Sci. Lett.* **52**, 227–238.

Carlson, R.W., Lugmair, G.W., 1988. The age of ferroan anorthosite 60025: oldest crust on a young Moon. *Earth Planet. Sci. Lett.* **90**, 119–130.

Eugster, O., Niedermann, S., Burger, M., Krähenbühl, U., Weber H., Clayton R., Mayeda T., 1989. Preliminary report on the Yamato-86032 lunar meteorite: III ages, noble gas isotopes, oxygen isotopes and chemical abundances. In: *Proceedings of the 2nd NIPR Symposium on Antarctic Meteorites*, pp. 25–35.

Eugster, O., 1989. History of meteorites from the Moon collected in Antarctica. *Science* **245**, 1197–1202.

Eugster, O., Terribilini, D., Polnau, E., Kramers, J., 2001. The antiquity indicator argon-40/argon-36 for lunar surface samples calibrated by uranium-235–xenon-136 dating. *Meteorit. Planet. Sci.* **36**, 1097–1115.

Eugster, O., Michel, T., 1995. Common asteroid break-up events of eucrites, diogenites, and howardites and cosmic-ray production rates for noble gases in achondrites. *Geochim. Cosmochim. Acta* **59**, 177–199.

Fukuoka, T., Laul, J.C., Smith, M.R., Schmitt, R.A., 1986. Chemistry of Yamato-82192 and -82193 (abstract). In: *Papers Presented to the 11th Symposium on Antarctic Meteorites*, pp. 40–42.

Fukuoka, T., Laul, J.C., Schmitt, R.A., 1989. Chemistry of Yamato-86032 lunar meteorite (abstract). In: *Papers Presented to the 14th Symposium on Antarctic Meteorites*, pp. 11–12.

Garrison, D., Hamlin, S., Bogard, D., 2000. Chlorine abundances in meteorites. *Meteorit. Planet. Sci.* **35**, 419–429.

Hartmann, W.K., 2003. Megaregolith evolution and cratering cataclysm models—lunar cataclysm as a misconception (28 years later). *Meteorit. Planet. Sci.* **38**, 579–593.

Haskin, L.A., Shih, C.-Y., Bansal, B.M., Rhodes, J.M., Wiesmann, H., Nyquist, L.E., 1974. Chemical evidence for the origin of 76535 as a cumulate. In: *Proceedings of the 5th Lunar Planetary Science Conference*, pp. 1275–1296.

Haskin, L.A., Lindstrom, M.M., Salpas, P.A., Lindstrom, D.J., 1981. On compositional variations among lunar anorthosites. *Proc. Lunar and Planet. Sci.* **12B**, 41–66.

James, O., 1980. Rocks of the early lunar crust. In: *Proceedings of the 11th Lunar Planetary Science Conference*, pp. 365–393.

Kaneoka, I., Takaoka, N., 1987. $^{40}$Ar–$^{39}$Ar analyses of lunar anorthositic breccia Yamato-82192. *Mem. Natl. Inst. Polar Res. Spec. Issue* **46**, 105–112.

Kaneoka, I., Nagao, K., 1993. $^{40}$Ar–$^{39}$Ar analyses of a lunar meteorite (Yamato-86032). In: *Proceedings of the 6th NIPR Symposium on Antarctic Meteorites*, pp. 88–99.

Karouji, Y., Ebihara, M., Yamaguchi, A., 2004. Chemical characteristics of lunar meteorites, Yamato 86032 and Dhofar 489 (abstract). *Antarct. Meteorit.* **XXVIII**, pp. 29–30.

Kieffer, S.W., Simonds, C.H., 1980. The role of volatiles and lithology in the impact cratering process. *Rev. Geophys. Space Phys.* **18**, 143–181.

Koeberl, C., 1988. Trace element geochemistry of lunar meteorites Yamato-791197 and -82192. In: *Proceedings of the 1st NIPR Symposium on Antarctic Meteorites*, pp. 122–134.

Koeberl, C., Warren, P.H., Lindstrom, M.M., Spettel, B., Fukuoka, T., 1989. Preliminary examination of the Yamato-86032 lunar meteorite: II. Major and trace element chemistry. In: *Proceedings of the 2nd NIPR Symposium on Antarctic Meteorites*, pp. 15–24.

Korotev, R.L., Jolliff, B.L., Rockow, K.M., 1996. Lunar meteorite Queen Alexandra Range 93069 and the iron concentration of the lunar highlands surface. *Meteorit. Planet. Sci.* **31**, 909–924.

Korotev, R.L., Jolliff, B.L., Zeigler, R.A., Gillis, J.J., Haskin, L.A., 2003a. Feldspathic lunar meteorites and their implications for compositional remote sensing of the lunar surface and the composition of the lunar crust. *Geochim. Cosmochim. Acta* **67**, 4895–4923.

Korotev, R.L., Jolliff, B.L., Zeigler, R.A., Gillis, J.J., Haskin, L.A., 2003b. Feldspathic lunar meteorites and their implications for compositional remote sensing of the lunar surface and the composition of the lunar crust. *Geochim. Cosmochim. Acta* **67**, 4895–4923.

Korotev, R.L., 2005. Lunar geochemistry as told by lunar meteorites. *Chemie der Erde* **65**, 297–346.

Krahenbuhl, U., Ganapathy, R., Morgan, J.W., Anders, E., 1973. Volatile elements in Apollo 16 samples: implications for highland volcanism and accretion history of the moon. In: *Proceedings of the 4th Lunar Planetary Science Conference*, pp. 1325–1348.

Jacobsen, S.B., Wasserburg, G.J., 1984. Sm–Nd isotopic evolution of chondrites and achondrites, II. *Earth Planet. Sci. Lett.* **67**, 137–150.

Lindstrom, M.M., Lindstrom, D.J., 1986. Lunar granulites and their precursor anorthositic norites of the early lunar crust. In: *Proceedings of the 16th Lunar Planetary Science Conference*, pp. D263–D276.

Lindstrom, M.M., Mittlefehldt, D.W., Martinez, R.R., Lipschutz, M.E., Wang, M.-S., 1991. Geochemistry of Yamato-82192, -86032 and -793274 lunar meteorites. In: *Proceedings of the 4th NIPR Symposium on Antarctic Meteorites*, pp. 12–32.

Lingenfelter, R.E., Canfield, E.H., Hampel, V.E., 1972. *Earth and Planetary Science Letters* **16**, 355–369.

Lorenzetti, S., Busemann, H., Eugster, O., 2005. Regolith history of lunar meteorites. *Meteorit. Planet. Sci.* **40**, 315–327.

McCallum, I.S., Mathez, E.A., 1975. Petrology of noritic cumulates and a partial melting model for the genesis of Fra Mauro basalts. In: *Proceedings of the 6th Lunar Planetary Science Conference*, pp. 395–414.

McDougall, I., Harrison, T.M., 1999. *Geochronology and thermochronology by the $^{40}Ar/^{39}Ar$ method*, 2nd ed. Oxford University Press, New York.

McKay, D.S., Bogard, D.D., Morris, R.V., Korotev, R.L., Johnson P., Wentworth, S.J., 1986. Apollo 16 regolith breccias: characterization and evidence for early formation in the mega-regolith. In: *Proceedings of the 16th Lunar Planetary Science Conference*, pp. D277–D303.

Norman, M.D., Borg, L.E., Nyquist, L.E., Bogard, D.D., 2003. Chronology, geochemistry, and petrology of a ferroan noritic anorthosite clast from Descartes breccia 67215: clues to the age, origin, structure, and impact history of the lunar crust. *Meteorit. Planet. Sci.* **38**, 645–661.

Nyquist, L.E., Hubbard, N.J., Gast, P.W., Bansal, B.M., Wiesmann, H., Jahn, B., 1973. Rb–Sr systematics for chemically defined Apollo 15 and 16 materials. In: *Proceedings of 4th Lunar Sciences Conferences, Geochim. Cosmochim. Acta*, Suppl. 4, **2**, pp. 1889–1914.

Nyquist, L.E., Bansal, B.M., Wiesmann, H., Jahn, B.-M., 1974. Taurus–Littrow chronology: some constraints on early lunar crustal development. In: *Proceedings of 5th Lunar Science Conference, Geochim. Cosmochim. Acta*, Suppl. 5, **2**, pp. 1515–1539.

Nyquist, L.E., Reimold, W.U., Bogard, D.D., Wooden, J.L., Bansal, B.M., Wiesmann, H., Shih, C.-Y., 1981. A comparative Rb–Sr, Sm–Nd, and K–Ar study of shocked norite 78236: evidence of slow cooling in the lunar crust? *Proc. Lunar Sci.* **12B**, 67–97.

Nyquist, L.E., Takeda, H., Bansal, B.M., Shih, C.-Y., Wiesmann, H., Wooden, J.L., 1986. Rb–Sr and Sm–Nd internal isochron ages of a subophitic basalt clast and a matrix sample from the Y75011 eucrite. *J. Geophys. Res.* **91**, 8137–8150.

Nyquist, L.E., Bogard, D.D., Wiesmann, H., Bansal, B.M., Shih, C.-Y., Morris, R.M., 1990. Age of a eucrite clast from the Bholghati howardite. *Geochim. Cosmochim. Acta* **54**, 2197–2206.

Nyquist, L.E., Wiesmann, H., Bansal, B., Shih, C.-Y., Keith, J.E., Harper, C.L., 1995. $^{146}$Sm–$^{142}$Nd formation interval for the lunar mantle. *Geochim. Cosmochim. Acta* **59**, 2817–2837.

Nyquist, L.E., Bogard, D.D., Shih, C.-Y., 2001. Radiometric chronology of the Moon and Mars. In: Bleeker, J., Geiss, J., Huber, M. (Eds.), *The Century of Space Science*. Kluwer Academic Publishers, Dordrecht, Holland, pp. 1325–1376.

Nyquist, L.E., Bogard, D.D., Shih, C.-Y., Wiesmann, H., 2002. Negative $\varepsilon_{Nd}$ in anorthositic clasts in Yamato 86032 and MAC88105: evidence for the LMO? (abstract) *Lunar Planet. Sci.* **33**, 1289, (CD-ROM).

Nyquist, L.E., Shih, C.-Y., Takeda, H., 2004. Chronology of eucrite petrogenesis from Sm–Nd and Rb–Sr systematics. *Antarct. Meteorit.* **XXVIII**, 66–67.

Nyquist, L.E., Yamaguchi, A., Bogard, D., Shih, C.-Y., Reese, Y., Takeda, H., 2005. Feldspathic clasts in Yamato 86032: remnants of a feldspathic lunar crust 4.4 Ga ago. *Antarct. Meteorit.* **XXIX**, 57–58.

Palme, H., Spettel, K., Jochum, K.P., Dreibus, G., Weber, H., Weckwerth, G., Wänke, H., Bischoff, A., Stöffler, D., 1991. Lunar highland meteorites and the composition of the lunar crust. *Geochim. Cosmochim. Acta* **55**, 3105–3122.

Ridley, W.I., Hubbard, N.J., Rhodes, J.M., Weismann, H., Bansal, B., 1973. The petrology of lunar breccia 15445 and petrogenetic implications. *J. Geol.* **81**, 621–631.

Russ III, G.P., Burnett, D.S., Lingenfelter, R.E., Wasserburg, G.J., 1971. Neutron capture on $^{149}$Sm in lunar samples. *Earth Planet. Sci. Lett.* **13**, 53–60.

Ryder, G., 2002. Mass flux in the ancient Earth–Moon system and benign implications for the origin of life on Earth. *J. Geophys. Res.* **107**, E4, 10.1029..

Shih, C.-Y., Nyquist, L.E., Dasch, E.J., Bogard, D.D., Bansal, B.M., Wiesmann, H., 1993. Ages of pristine noritic clasts from lunar breccias 15445 and 15455. *Geochim. Cosmochim. Acta* **57**, 915–931.

Shih, C.-Y., Nyquist, L.E., Reese, Y., Yamaguchi, A., Takeda, H., 2005. Rb–Sr and Sm–Nd isotopic studies of lunar highland meteorite Y-86032 and lunar ferroan anorthosites 60025 and 67075. In: *Lunar Planetary Science*, **XXXVI**, Abstract #1433, Lunar and Planetary Institute, Houston (CD ROM).

Stoenner, R.W., Schaeffer, O.A., Katcoff, S., 1965. Half-lives of argon-37, argon-39, and argon-42. *Science* **148**, 1325–1328.

Stöffler, D., 1981. Cratering mechanics: data from terrestrial and experimental craters and implications for the Apollo 16 site (abstract). In: James, O.B., Hörz, F., *Workshop on Apollo 16*, LPI Tech. Rpt. 81-01, pp. 132–141.

Takaoka, N., Yosida, Y., 1992. Noble gases in Yamato-793274 and -86032 lunar meteorites. *Proc. NIPR Symp. Antarct. Meteorit.* **5**, 36–48.

Takeda, H., Kojima, H., Nishio, F., Yanai, K., Lindstrom, M. M., Yamato Lunar Meteorite Consortium Group, 1989. Preliminary report on the Yamato-86032 lunar meteorite: I. Recovery, sample descriptions, mineralogy and petrography. In: *Proceedings of the 2nd NIPR Symposium on Antarctic Meteorites*, pp. 3–14.

Takeda, H., Mori, H., Tagai, T., 1987. Mineralogy of lunar meteorites, Yamato-82192 and -82193 with reference to breccias in a breccia. *Mem. Natl. Inst. Polar Res., Spec. Issue* **46**, 43–55.

Takeda, H., Miyamoto, M., Mori, H., Wentworth, S.J., McKay, D.S., 1990. Mineralogical comparison of the Y-86032-type lunar meteorites to feldspathic fragmental breccia 67016. *Proc. Lunar Planet. Sci. Conf.* **20**, 91–100.

Takeda, H., Nyquist, L. E., Kojima, H., 2002. Mineralogical study of a gray anorthositic clast in the Yamato 86032 lunar meteorite: windows to the far-side highland (abstract). *Lunar Planet. Sci.*, **33**, 1267 (CD-ROM).

Takeda, H., Yamaguchi, A., Bogard, D.D., Karouji, Y., Ebihara, M., Ohtake, M., Saiki, K., Arai, T., 2006. Magnesian anorthosites and a deep crustal rock from the farside crust of the moon. *Earth Planet. Sci. Lett.* **247**, 171–184.

Tatsumoto, M., Premo, W.R., 1991. U–Pb isotopic characteristics of lunar meteorites Yamato-793274 and Yamato-86032. In: *Proceedings of the 4th NIPR Symposium on Antarctic Meteorites*, pp. 56–69.

Tera, F., Papanastassiou, D.A., Wasserburg, G.J., 1974. Isotopic evidence for a terminal lunar cataclysm. *Earth Planet. Sci. Lett.* **22**, 1–21.

Tompkins, S., Pieters, C.M., 1999. Mineralogy of the lunar crust: results from clementine. *Meteorit. Planet. Sci.* **34**, 25–41.

Turner, G., Cadogan, P.H., Yonge, C.J., 1973. Argon selenochronology. In: *Proceedings of 4th Lunar Science Conference, Geochim. Cosmochim. Acta*, Suppl. 4, **2**, pp. 1889–1914.

Vogt, S., Fink, D., Klein, J., Middleton, R., Dockhorn, B., Korschinek, G., Nolte, E., Herzog, G.F., 1991. Exposure histories of the lunar meteorites: MAC88104, MAC88105, Y791197, and Y86032. *Geochim. Cosmochim. Acta* **55**, 3157–3165.

Walker, D., 1983. Lunar and terrestrial crust formation. *Proc. Lunar Planet. Sci. Conf.* **14**, B17–B25.

Warren, P.H., Kallemeyn, G.W., 1991. Geochemical investigation of five lunar meteorites: Implications for the composition, origin and evolution of the lunar crust. In: *Proceedings of the 4th NIPR Symposium on Antarctic Meteorites*, pp. 91–117.

Warren, P.H., Wasson, J.T., 1977. Pristine nonmare rocks and the nature of the lunar crust. *Proc. Lunar Planet. Sci. Conf.* **8**, 2215–2235.

Wasserburg, G.J., Jacobsen, S.B., DePaolo, D.J., McCulloch, M.T., Wen, T., 1981. Precise determination of the Sm/Nd ratios, Sm and Nd isotopic abundances in standard solutions. *Geochim. Cosmochim. Acta* **45**, 2311–2323.

Yamaguchi, A., Takeda, H., Nyquist, L.E., Ebihara, M., Karouji, Y., 2004. The origin and impact history of lunar meteorite.

Yamaguchi, A., Takeda, H., Karouji, Y., Ebihara, M., Nyquist, L.E., Bogard, D.D., Shih, C.-Y., Reese, Y., 2005. Yamato-86032 lunar meteorite: implications for impact history of the highland crust (abstract). *Antarct. Meteorit.* **XXIX**, pp. 96–97.